frontiers | Frontiers in Marine Science

TYPE Original Research
PUBLISHED 16 October 2023
DOI 10.3389/fmars.2023.1215048

OPEN ACCESS

EDITED BY
Xu Zhang,
Chinese Academy of Sciences (CAS), China

REVIEWED BY
Xuyuan Ai,
Max Planck Institute for Chemistry, Germany
Yunhai Li,
Ministry of Natural Resources, China

*CORRESPONDENCE
Xibin Han
hanxibin@sio.org.cn

RECEIVED 01 May 2023
ACCEPTED 25 September 2023
PUBLISHED 16 October 2023

CITATION
Hu L, Zhang Y, Wang Y, Ma P, Wu W, Ge Q, Bian Y and Han X (2023) Paleoproductivity and deep-sea oxygenation in Cosmonaut Sea since the last glacial maximum: impact on atmospheric CO_2. *Front. Mar. Sci.* 10:1215048. doi: 10.3389/fmars.2023.1215048

Paleoproductivity and deep-sea oxygenation in Cosmonaut Sea since the last glacial maximum: impact on atmospheric CO_2

Liangming Hu[1,2], Yi Zhang[1,2], Yizhuo Wang[3], Pengyun Ma[4], Wendong Wu[5], Qian Ge[1,2], Yeping Bian[1,2] and Xibin Han[1,2]*

[1]Key Laboratory of Submarine Geosciences, Ministry of Natural Resources, Hangzhou, China, [2]Second Institute of Oceanography, Ministry of Natural Resources, Hangzhou, China, [3]Institute of Sedimentary Geology, Chengdu University of Technology, Chengdu, China, [4]College of Geodesy and Geomatics, Shandong University of Science and Technology, Qingdao, China, [5]School of Mechanical Engineering, Shanghai Jiao Tong University, Shanghai, China

The paleoproductivity in the Southern Ocean plays a crucial role in controlling the atmospheric CO_2 concentration. Here, we present the sediment record of gravity core ANT37-C5/6-07, which was retrieved from the Cosmonaut Sea (CS), Indian Ocean sector of the Southern Ocean. We found that the change in the oxygen concentration in the CS bottom water is strongly correlated with the atmospheric CO_2 fluctuations since the Last Glacial Maximum (LGM). Based on the change in the export production, we reconstructed the evolution history of the deep-water ventilation/upwelling in the study area. During the LGM, a large amount of respiratory carbon was stored in the deep Southern Ocean due to the effect of the low export productivity and restricted ventilation. The oxygen concentration was also low at this time. Despite the increase in paleoproductivity, the biological pump efficiency remained at a low level during the Last Deglaciation. Vast quantities of CO_2 were released into the atmosphere through enhanced upwelling. The recovery of ventilation during this period facilitated the supply of oxygen-rich surface water to the deep ocean. Moreover, signals were identified during the transitions between the Heinrich Stage 1 (HS1), Antarctic Cold Reverse (ACR), and Younger Drays (YD) periods. During the Holocene, the productivity increased overall, and the oxygen in the bottom water was consumed but still remained at a high level. This may have been caused by the enhanced ventilation and/or the prevalence of East Cosmonaut Polynya (ECP) near Cape Ann.

KEYWORDS

paleoproductivity, oxygenation, last glacial maximum, carbon cycling, Cosmonaut Sea

1 Introduction

The Southern Ocean covers approximately 20% of the global ocean area, accounts for 30–40% of the global oceanic net CO_2 absorption and serves as an important carbon sink region (Gao et al., 2001). The Southern Ocean could exert a substantial control on the partial pressure of CO_2, due to its leverage on the efficiency of the global soft-tissue pump through which the photosynthetic production, sinking and remineralization of organic matter store dissolved inorganic carbon (DIC) in the ocean's interior (Sarmiento and Nicolas, 2006; Jaccard et al., 2016). The atmosphere-ocean carbon cycle is inextricably linked to ocean production in all sectors and at all times (Jaccard et al., 2005; Sigman et al., 2010). In the southern part of the Antarctic Polar Front, the surface productivity tends to decrease during cold periods and increase during warm periods (Bonn et al., 1998; Anderson et al., 2009). Marine primary productivity refers to the ability of marine upper plankton to convert inorganic carbon into organic carbon (Raynaud et al., 1992; Graham et al., 2015). By studying marine paleoproductivity, we can gain insights into the CO_2 exchange between the ocean and atmosphere, providing a better understanding of the biogeochemical cycle of carbon in atmosphere-ocean-benthic sediment systems (Paytan et al., 1996; Lin et al., 1999).

Previous research has established that marine diatoms are responsible for the majority of the primary production in the Southern Ocean (DeMaster et al., 1991). As the primary producer in Antarctic coastal waters, diatoms assimilate dissolved Si and CO_2 in water for growth, consequently providing over 75% of the Southern Ocean's export productivity (Quéguiner et al., 1991; Nelson et al., 1995). Silica productivity in seawater mainly consists of biogenic opal and organic matter (Bonn et al., 1998). Following their demise, the remains of diatoms detach from the surface seawater and sink to the seafloor, making Si a crucial component in governing the carbon cycle in the Southern Ocean (Tréguer, 2002). Biogenic silicon is a valuable proxy and is closely associated with climatic conditions (Armand et al., 2005; Crosta et al., 2005; Esper et al., 2010; Esper and Gersonde, 2014a; Esper and Gersonde, 2014b). Hence, it is widely used in the studies of paleoproductivity and the carbon cycle in the Southern Ocean (Agnihotri et al., 2008; Hu et al., 2022). Moreover, the exportation, sedimentation, and preservation of biogenic silicon are closely related to the occurrence of marine barite ($BaSO_4$) in sediments, and there is a strong correlation between the accumulation of biogenic barium and the carbon output to the deep sea (Dymond et al., 1992). Consequently, researchers have conducted many investigations on the paleoproductivity in the Southern Ocean, using biogenic barium as an alternative indicator (Dehairs et al., 1991; Bonn et al., 1998; Fagel et al., 2002).

Reconstructing changes in bottom water oxygenation in the past can provide a better understanding of the relevant processes. The remineralization of organic matter leads to significant changes in the dissolved oxygen concentration, in conjunction with variations in respiratory carbon storage (Hoogakker et al., 2015; Jaccard et al., 2016; Jacobel et al., 2017; Anderson et al., 2019). The temporal evolution of bottom water oxygenation can be reconstructed qualitatively using the distribution of redox-sensitive metals in marine sediments (Calvert and Pedersen, 1996; Nameroff et al., 2002). Enhanced ventilation, particularly in high-latitude regions, plays a significant role in the provision and recovery of the oxygen content in deep ocean layers (Schmittner et al., 2008; Ridgwell and Schmidt, 2010; Amsler et al., 2022). As a result, identifying the redox environment in the deep Southern Ocean is essential to understanding the changes in deep-sea ventilation and surface water productivity (Pailler et al., 2002; Li et al., 2010; Jaccard et al., 2016).

While previous studies have gained a regionally integrated understanding of the leverage the Southern Ocean bears on the air-sea partitioning of CO_2 across the last deglacial termination, observations are largely based on records from the southern Atlantic. Records from the Pacific and Indian sectors of the Southern Ocean are consistent with the first-order paleoceanographic evolution, but regional specificities exist. In particular, it remains unclear how export production patterns vary regionally in the Indian sector of the Southern Ocean, and they are characterized by a complex frontal structure (Durgadoo et al., 2008).

Based on the connections to the global ocean, the overturning circulation of the Southern Ocean has been usefully separated into "upper" and "lower" cells (Toggweiler et al., 2006). Previous studies in the Indian Ocean sector focused on the SAZ and the AZ near the Polar Front and reflected the changes in the upper cell of the Southern Ocean ventilation (Ai et al., 2020; Sigman et al., 2021; Amsler et al., 2022). Based on five sediment cores encompassing the Subantarctic and Antarctic zones in the southwestern Indian Ocean, Amsler et al. (2022) argued that regional changes in the export of siliceous phytoplankton to the deep sea may have entailed a secondary influence on oxygen levels at the water–sediment interface, especially in the SAZ near the Polar Front. Although these records highlight the role that the Indian Ocean sector played in the air–sea partitioning of CO_2 on glacial–interglacial timescales, they are still insufficient to reveal the impact of the lower cell, which ventilates the deeper limb of the Southern Ocean's overturning circulation. In the western Cosmonaut Sea, recent studies were conducted by Hu et al. (2022) and Li et al. (2021). Based on a study of core ANT36-C4-05, Hu et al. (2022) argued that the paleoproductivity of the Cosmonaut Sea has fluctuated strongly since the Middle Holocene, and its evolution trend is basically consistent with the temperature change in the Antarctica, which is greatly restricted by the change in the sea ice range. Li et al. (2021) compared the diatom data for two cores from the western Cosmonaut Sea to other records from the Southern Ocean to reveal the climatic response of the ice-proximal environment to the melting of the ice sheet from the Last Glacial Maximum (LGM) to the Holocene. Both investigations were carried out in the Antarctic Zone of the Cosmonaut Sea, far from the coast.

Based on the baseline research on oceanography, krill, and the environment-West (BROKE-West) survey, Westwood et al. (2010) reported that the rate of primary productivity was significantly higher within the marginal ice zone compared to the open ocean.

The region between 50°E and 60°E has been reported to be a region of converging flow because the Antarctic Slope Current (ASC) is directed northwestward by the topography along the Mawson Coast and meets the Antarctic Circumpolar Current (ACC) north of Cape Ann (Williams et al., 2010). Based on observational and satellite data, Anilkumar et al. (2014) found that the Chl *a* content is high in the coastal region between 52°E and 60°E, with the maximum occurring between 52°E and 54°E. This region is located in the southern part of the ACC, making it an important upwelling region associated with the atmospheric Antarctic Divergence (Williams et al., 2010). Since the upwelling caused by the Antarctic Divergence draws circumpolar deep water (CDW) into the surface waters, it is sometimes co-located with the southern boundary (SB) of the ACC. This upwelling feature is thought to be associated with increased biological activity in all trophic levels (Nicol and Foster, 2003). Moreover, the region offshore of Cape Darnley immediately to the west has high oxygen concentrations and bottom-intensified flows, suggestive of local bottom-water formation that can extend westward to ~30°E (Meijers et al., 2010).

Overall, the productivity in the Cosmonaut Sea coastal region north of Cape Ann has significant regional characteristics and is closely related to the lower layer of the circulation system in the Indian Ocean sector. There is great potential in using the sedimentary records of the Cosmonaut Sea since the LGM to learn about the evolution of climate-driven biogeochemistry. In this study, we established a chronological framework for the top segment of core ANT37-C5/6-07. Based on suitable proxies of paleoproductivity and bottom-water oxygenation, we aimed to reconstruct the co-evolution of the paleoproductivity and deep-water ventilation in the Cosmonaut Sea since the LGM and to reveal their impact and feedback on the carbon cycle in the Indian Ocean sector of the Southern Ocean.

2 Regional setting

The Cosmonaut Sea is part of the Indian Ocean sector of the Southern Ocean, spanning 30–60°E. It is bordered by the Enderby Land to the south, the Cooperation Sea to the east, and the Gunnerus Ridge to the west, and it is adjacent to the Riiser-Larsen Sea (Figure 1) (Hu et al., 2022). There are mainly three small bays along the coast, namely, the Amundsen Bay, the Casey Bay, and the Lützow-Holm Bay from east to west. The Cosmonaut Sea is located in the middle of two large bays, the Weddell Bay and the Prydz Bay, which create two major circulation systems around the study area, the East Weddell Gyre and the Prydz Bay Gyre, respectively (Heywood et al., 1999; Meijers et al., 2010). The bottom edge of the Amery Ice Shelf in the Prydz Bay may extend to the area near the eastern coast of the Cosmonaut Sea (Wong et al., 1985).

The ocean current system in the Cosmonaut Sea area exhibits a complex pattern (Hu et al., 2022). The region has three distinct banded fronts: the southern front of the ACC (sACCf), the SB, and the Antarctic Slope Front (ASF) from north to south (Meijers et al., 2010). The ASF is effectively the result of the deepening of the T_{min} layer over the upper continental slope toward the shelf break (Williams et al., 2010). A strong westward current, associated with the horizontal pressure gradient of the ASF, is referred to as the Antarctic Slope Current (ASC). The main feature of the ASC is a strong jet that is generally located over the upper continental slope at depths of 750–1250 m. The surface circulation consists of the eastward flowing ACC and the westward flowing Antarctic Coastal Current (CC) (Figure 1). The Antarctic Coastal Current flows westward through the Cosmonaut Sea from the Prydz Bay, forming two branches at the Gunnerus Ridge. One continues westward, while the other branch creates an anticyclonic circulation that deflects to the northeast (Bibik et al., 1988).

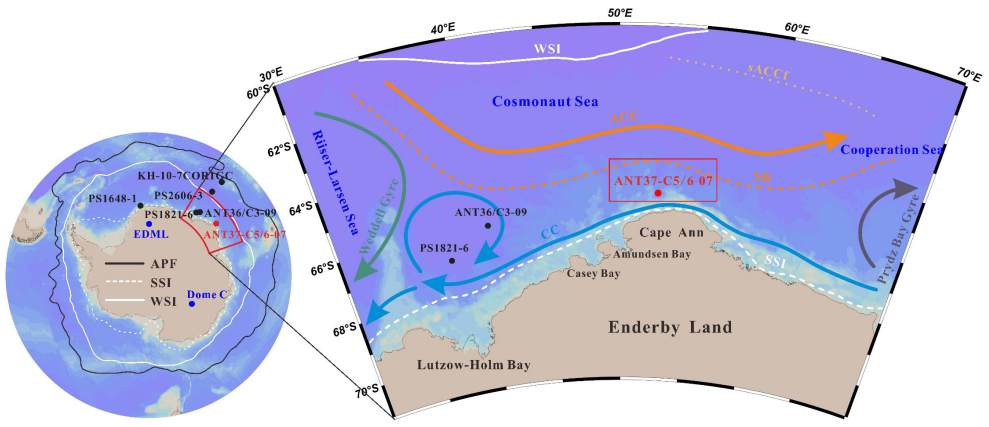

FIGURE 1
Regional setting and locations of the studied and referenced cores. The black solid line indicates the location of the Antarctic Polar Front (APF) (Orsi et al., 1995). The white solid line and the white dashed line indicate the average extent of the modern winter sea ice (WSI) and summer sea ice (SSI), respectively (Comiso, 2003). The ocean circulation patterns of the Antarctic Circumpolar Current (ACC) and the coastal current (CC) are indicated by the orange and blue arrows, respectively (modified after Hunt et al., 2007). The green and gray arrows indicate the Weddell Gyre and the Prydz Bay Gyre, respectively (modified after Hu et al., 2022). The golden dotted line indicates the southern front of the ACC (sACCf) (Hu et al., 2022). The southern boundary of the ACC (SB) is denoted by the orange dashed line (Hunt et al., 2007). The red rectangle represents the position of the ECP (Comiso and Gordon, 1996).

The ACC predominantly consists of the CDW, which is transported eastward around Antarctica, connecting the Atlantic, Indian, and Pacific oceans (Williams et al., 2010). The lower CDW originates from North Atlantic Deep Water, while the upper CDW consists of Indian Deep Water and Pacific Deep Water (Talley, 2013). The Southern Ocean also has a meridional overturning circulation that transports the CDW southward toward the Antarctic continental slope where it shoals and is transformed into cold and fresh Antarctic surface water (AASW). Part of the ACC water mass mixes with the shelf water near the front edge of the continental shelf in the eastern Cosmonaut Sea (Bibik et al., 1988; Klyausov and Lanin, 1988). The dense shelf water sinks off Cape Darnley, forming the Cape Darnley bottom water (CDBW), which contributes to the Antarctic bottom water (AABW) (Aoki et al., 2020). Based on lowered-acoustic Doppler current profiler (LADCP) data, Meijers et al. (2010) reported the occurrence of westward-flowing AABW high on the continental slope. This westward-flowing region at the bottom has been found to become progressively deeper and covers our sampling point.

The East Antarctic Ice Sheet was relatively stable during the Last Deglaciation, so, the Cosmonaut Sea was mainly affected by the melt water from the West Antarctic Ice Sheet (Li et al., 2021). Previous studies have pointed out that winter sea ice (WSI) can extend northward to 60°S, while the range of the summer sea ice (SSI) in the Indian Ocean zone of the Southern Ocean has remained relatively unaltered from the LGM to the present day (Gersonde et al., 2005). Based on more than 20 years of satellite observation data, Comiso and Gordon (1996) reported a long-lasting polynya near Cape Ann in the Cosmonaut Sea. Polynyas are areas of persistent open water or reduced ice concentration surrounded by sea ice (Smith et al., 1990; Morales Maqueda et al., 2004). The West Cosmonaut Polynya (WCP) occurs west of 45°E, which is formed by storms. The east polynya, located in the coastal region north of Cape Ann, is known as the East Cosmonaut Polynya (ECP) (Prasad et al., 2005). Previous studies have suggested that ocean forcing and/or divergent winds may have contributed to the formation of the ECP (Comiso and Gordon, 1996; Arbetter et al., 2004; Bailey et al., 2004).

3 Materials and methods

3.1 Sample collection

Gravity core ANT37-C5/6-07 was obtained off the coast of Cape Ann (65°21.27'S, 52°35.69'E) in the Cosmonaut Sea during the 37th Chinese Antarctica Expedition. The core site is located north of the modern SSI and south of the WSI range. Cape Ann is the northernmost promontory on the Antarctic continent where the surfaces of Antarctic glaciers reach, except for the Antarctic Peninsula (Comiso and Gordon, 1996). The sampling point is located on the continental ridge at a water depth of 2825 m. The top of the core is shown as grayish olive green, and the lithology is dominated by clayey silt. As shown in the X-radiographic image (Figure 2), there is no obvious sedimentary hiatus in the core. The entire core was divided into four segments with similar lengths. The first segment at the top (length of 91 cm) was used in this study.

3.2 Dating

Reliably dating glaciomarine sediments deposited on the Antarctic shelf since the LGM is challenging due to the scarcity of calcareous (micro-) fossils and the recycling of fossil organic matter. Therefore, accelerator mass spectrometry (AMS) ^{14}C-dating is commonly performed on the acid-insoluble organic fraction (AIO) of marine sediments (Licht and Andrews, 2002; Hillenbrand et al., 2010; Hu et al., 2022). The AIO primarily consists of diatomaceous organic matter, and

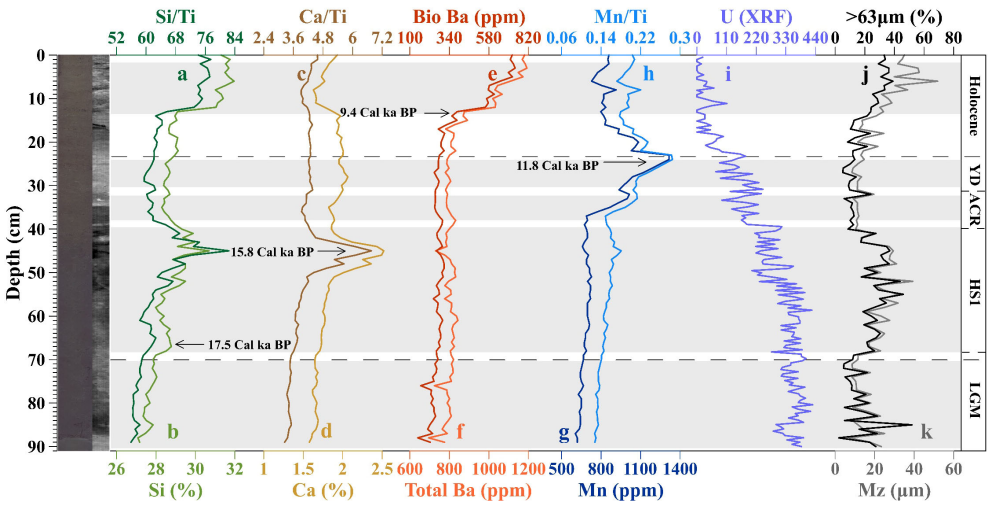

FIGURE 2
Downcore distribution patterns of the paleoproductivity proxies, oxygenation proxies, and the percentage of >63 μm grains in the core sediments. **(A)** Si/Ti ratios, **(B)** Si content, **(C)** Ca/Ti ratios, **(D)** Ca content, **(E)** Bio Ba content, **(F)** Total Ba content, **(G)** Mn content, **(H)** Mn/Ti ratios, **(I)** U (XRF) content, **(J)** percentage of >63 μm grains, and **(K)** mean grain size of core sediments.

it is assumed to provide reliable age models for sediment cores retrieved from the Southern Ocean (Licht and Andrews, 2002). We selected sediment samples from six layers (1 cm, 12 cm, 32 cm, 45 cm, 68 cm, and 91 cm) in the top segment and conducted radioactive ^{14}C-dating analysis of these samples at the Beta Analytic Testing Laboratory, Miami (Table 1).

3.3 Paleoproductivity proxies

The main elements in the bulk samples were analyzed via X-ray fluorescence spectrometry (XRF), while the trace elements were analyzed using an Elan DRC-e inductively coupled plasma mass spectrometry (ICP-MS) with a sampling resolution of 1 cm. The sediment grain size was determined using a Mastersizer 2000 analyzer. In addition, we also used an XRF core scanner (ITRAX) to collect optical and X-radiographic images and to obtain high-resolution element profiles of the core. Since only biogenic barium from discrete barite particles (associated with decaying organic matter) provides information on the export of organic matter to the seafloor, the impacts of barium from other sources must be eliminated (Dehairs et al., 1980; Dymond et al., 1992). Investigations of various sedimentary environments have shown that the main impact comes from terrigenous debris, which varies widely between 200 and 1000 ppm (Dymond et al., 1992; Gingele and Dahmke, 1994; Stroobants et al., 1991). A normative approach is commonly used to distinguish between detrital barium and biogenic barium (Bio Ba) (Dymond et al., 1992; Gingele and Dahmke, 1994). The correlation between Al and Ti in the samples is high (R^2 = 0.7894) (Figure 3E), and the downcore distribution patterns of both are highly consistent (Figures 3A, B), indicating the absence of significant biogenic Al. Therefore, the barium/aluminum ratio and the barium/titanium ratio were used for the correction of the debris end. The equations for calculating the biogenic barium content are as follows:

$$Bio\ Ba = Ba_{total} - Al_{sam} \times (Ba/Al)_{ter} \quad (1)$$

$$Bio\ Ba = Ba_{total} - Ti_{sam} \times (Ba/Ti)_{ter} \quad (2)$$

where Bio Ba denotes biogenic barium, and Ba_{total}, Al_{sam}, and Ti_{sam} are the total Ba, total Al, and total Ti contents in the sediment sample, respectively. $(Ba/Al)_{ter}$ and $(Ba/Ti)_{ter}$ are used to indicate the abundance of Ba in the continental crust. The Ba/Al ratio of aluminum silicate in the global crust is 0.005–0.01, the average value method was used to obtain a value of 0.0075 according to previous studies (Dymond et al., 1992; Hu et al., 2022). The $(Ba/Ti)_{ter}$ value is 0.126 (Turekian and Wedepohl, 1961). We assumed that the composition of the terrestrial materials related to the barium content was constant in time and space (Bonn et al., 1998). Figure 3 shows that there is no significant difference between the distribution patterns of Bio Ba calculated using $(Ba/Al)_{ter}$ and $(Ba/Ti)_{ter}$. However, the range of the Bio Ba values calculated using $(Ba/Al)_{ter}$ is closer to that obtained in a previous study in the Indian Ocean sector of the Southern Ocean (Figures 4G–I) (Bonn et al., 1998), so we chose to use the Bio Ba content obtained using Eq. (1).

In addition, we also used the ratios of Si and Ca to Ti to indicate changes in the paleoproductivity, thereby eliminating the impact of the terrigenous clastic input (Cheshire and Thurow, 2005; Agnihotri et al., 2008). Finally, we selected Bio Ba and Si/Ti as alternative proxies of the siliceous productivity, and Ca/Ti as an alternative proxy of biogenic calcium carbonate and the calcareous productivity.

3.4 Oxygenation proxies

The concentration of redox sensitive elements (RSEs) in sediments can reflect the oxygen content at the water-sediment interface and in bottom water and has been widely used as an alternative indicator of the redox environment in the deep ocean (Calvert and Pedersen, 1993; Brown et al., 2000). Under reducing or suboxidizing conditions, Mn is dissolved in water as ionic Mn(II). While under oxidizing conditions, it produces Mn oxides/hydroxides in the form of Mn(III) or Mn(IV), which are precipitated and enriched in the sediments (Calvert and Pedersen, 1993; Calvert and Pedersen, 1996). When the deposition environment becomes a suboxidizing or even anoxic environment again, the Mn hydroxide will be reduced to Mn(II) (Mn^{2+} or $MnCl^{+}$) and will migrate upward or downward in the sediment column (Middelburg et al., 1987; Brumsack, 1989; Morford et al., 2001). Another characteristic of Ti is that it is almost unaffected by changes in the redox conditions of seawater. We used the Mn/Ti ratio to eliminate the dilution effect of terrestrial debris components (Wang et al., 2018).

In oxygenated environments, uranium (U) is present as soluble U (VI). When the seawater becomes oxygen-depleted, the U is reduced and is precipitated as insoluble U(IV) in the form of

TABLE 1 AMS ^{14}C data and the calibrated calendar ages for the top 91 cm of core ANT37-C5/6-07.

Lab ID	Depth (cm)	Material	^{14}C age (a BP)	Calibrated age (a BP)	Old carbon age (a)	Calendar age (Cal a BP)
616427	0–1	Organic carbon	5300 ± 30	2118	2118	0
664982	11–12	Organic carbon	13230 ± 50	11486	2118	9368
664983	31–32	Organic carbon	18410 ± 60	18035	2118	15917
616428	44–45	Organic carbon	18210 ± 50	17774	2118	15656
664984	67–68	Organic carbon	19810 ± 80	19280	2118	17162
616430	90–91	Organic carbon	27830 ± 120	28116	2118	25998

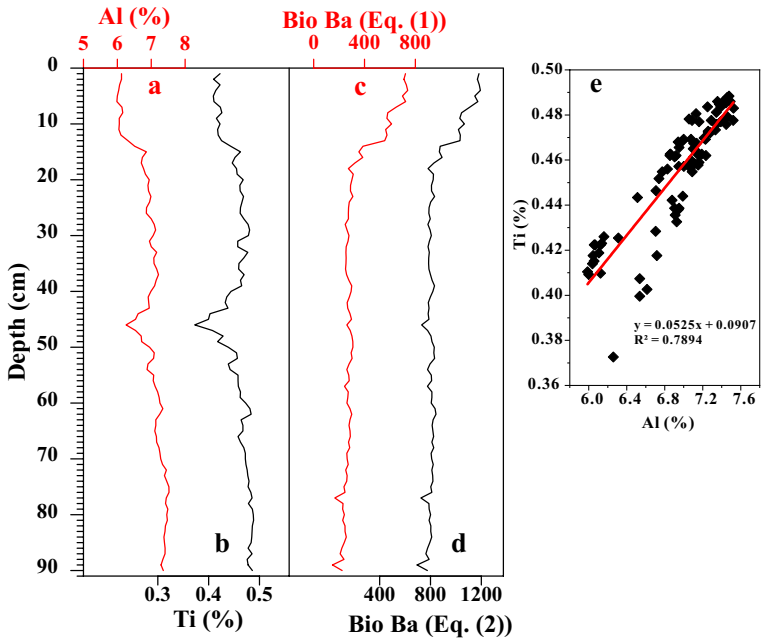

FIGURE 3
Effects of different Ba/Al and Ba/Ti ratios (Eqs. (1) and (2)) on computing the detrital barium background from the Batotal values. **(A)** Al content, **(B)** Ti content, **(C)** Bio Ba content (Eq. (1)), **(D)** Bio Ba content (Eq. (2)), and **(E)** the correlation between Ti (%) and Al (%) of core sediments.

uraninite (Morford and Emerson, 1999). Under reducing conditions, the decrease in the U concentration of the sediment porewater will create a concentration gradient between the bottom water and the uppermost sediment layers. This gradient leads to the diffusion of the dissolved U into the sediment and to the precipitation of authigenic U (aU) phases (Langmuir, 1978). And the authigenic fraction typically amounts for > 60% of the total U (Amsler et al., 2022). Therefore, the Mn/Ti ratio and U content (data collected from the XRF core scanner) were used as two proxies of the oxygenation of bottom water in this study.

4 Results

4.1 Chronology

The AMS ^{14}C dating results for the selected three layers are presented in Table 1. We found that an age reversal occurred at 32 cm. We speculate that at ~16 Cal ka BP, there may have been a sudden intensify of terrestrial material input, resulting in the interference of terrestrial-derived old carbon in this layer. The age model obtained after removing the data from this layer is consistent with that calculated through Bacon age-depth modelling tool, which indicates that this age reversal has a minimal impact on our study. Therefore, we rounded off the data for that layer. The test age was corrected using the Calib 8.2.0 (Stuiver and Reimer, 1993) procedure and the Marine 20 calibration dataset (Heaton et al., 2020). According to previous studies, a delta R value of 1120 for carbon storage correction was used (Yoshida and Moriwaki, 1979; Takano et al., 2012). After the correction and fitting, the corrected ages of the samples from the top segment of the core were obtained: 2118 Cal a BP at 1 cm and 28116 Cal a BP at 91 cm.

Similarly, AMS ^{14}C dating of the AIO from surface seafloor sediments around Antarctica has frequently yielded ages of several thousand years (Andrews et al., 1999; Pudsey et al., 2006). The occurrence of old surface ages combined with the potential error of downcore AIO ages complicates the reliability of ^{14}C-based age models for post-LGM sedimentary sequences south of the APF (Hillenbrand et al., 2010). Usually, down-core AIO ages are corrected by subtracting the age of the top of the core (Andrews et al., 1999; Pudsey et al., 2006). Hu et al. (2022) determined the downcore distribution pattern of $^{210}Pb_{ex}$ in the top 20 cm section of adjacent core ANT36-C4-05. They found that the specific activity of $^{210}Pb_{ex}$ decreased exponentially from the surface to a depth of 4 cm, and it fluctuated within the range of the background values below 4 cm. Therefore, the surface layer of the core is considered to be modern sediment, and the age of the top of the core is 0 Cal a BP. An age of 2118 a was used as the old carbon age for the correction in this study, and the final calendar ages of each layer were obtained after removing the influence of the old carbon storage (Table 1). After calculating the calendar age, we obtained the accumulation rate of the top 91 cm of the core (Figure 5). Our data are similar to those of a previous study of adjacent cores (Bonn, 1995).

4.2 Characteristics of the paleoproductivity proxies

As shown in Figure 2, during the LGM, the values of the alternative indicators of paleoproductivity fluctuated within narrow ranges and typically remained at a relatively low level.

In the early stage of the Last Deglaciation, there was no significant change in the Bio Ba value and Ca/Ti ratio (Figures 2C, E), while the Si/

10.3389/fmars.2023.1215048

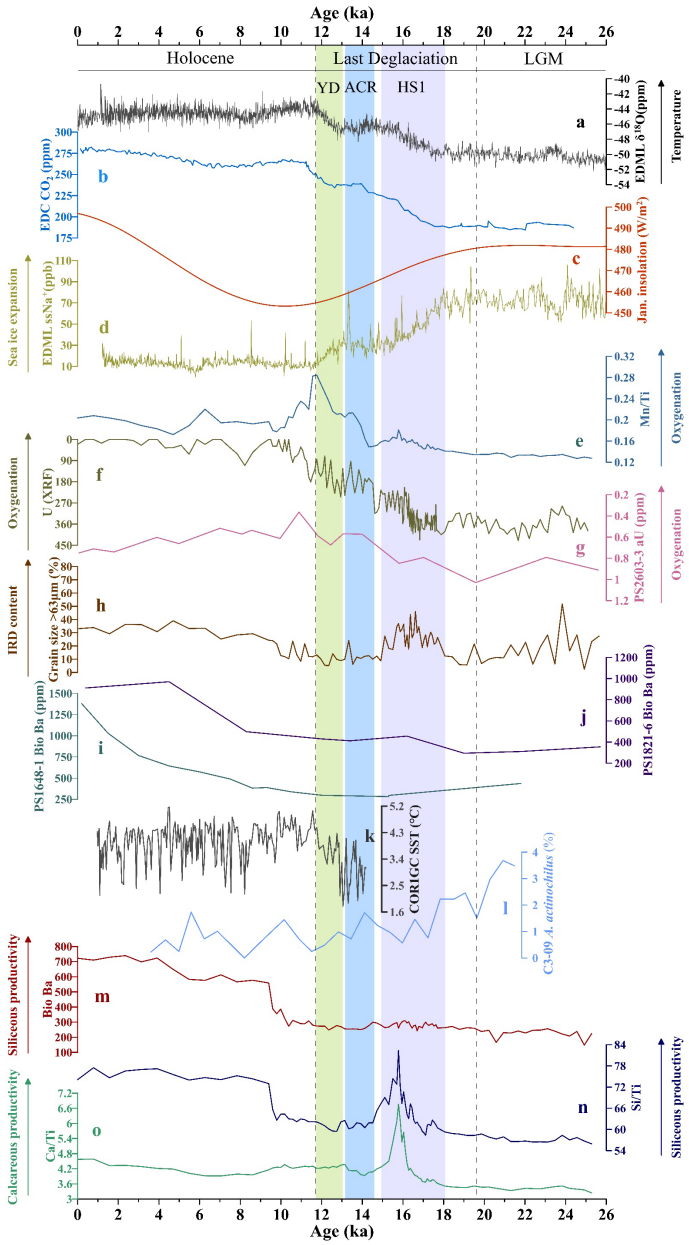

FIGURE 4
Comprehensive comparison of paleoproductivity and oxygenation proxies of our samples with records from ice cores and other sediment cores. **(A)** EDML $\delta^{18}O$ content (EpicaCommunityMembers, 2006), **(B)** EDC CO_2 content (Monnin et al., 2004; Schmitt et al., 2012), **(C)** summer insolation in the Southern Hemisphere at 65°S (Laskar et al., 2004), **(D)** EDML $ssNa^+$ content (Fischer et al., 2007), **(G)** authigenic uranium (aU) concentrations of core PS2603-3 (Amsler et al., 2022), **(I, J)** Bio Ba contents in cores PS1648-1 and PS1821-6 (Bonn, 1995), **(K)** sea surface temperature record of core KH-10-7COR1GC (Orme et al., 2020), **(L)** *Actinocyclus actinochilus* abundance of core ANT36/C3-09 (Li et al., 2021). **(E)** Mn/Ti ratios, **(F)** U content (XRF), **(H)** percentage of >63 μm grains, **(M)** Bio Ba content, **(N)** Si/Ti ratios, and **(O)** Ca/Ti ratios of core sediments.

Ti ratio exhibited a minor peak at ~19.1 Cal ka BP, followed by a decline before entering Heinrich Stage 1 (HS1, 18–14.6 Cal ka BP) (Figure 2A). During HS1 (corresponding to the W2 warm period in the Southern Hemisphere) (Siani et al., 2013), all of the paleoproductivity proxies exhibited increasing trends, but the Bio Ba curve remained relatively flat. The Si/Ti and Ca/Ti ratios reached high peaks in the middle stage of HS1 (~15.9 Cal ka BP), whereas the Bio Ba curve had a low value during this period. During the Antarctic Cold Reverse period (ACR, 13.1–14.7 Cal ka BP), all of the paleoproductivity proxies exhibited a decline to varying degrees, with the most significant reductions occurring in the Si/Ti and Ca/Ti ratios. After the ACR, the Ca/Ti curve exhibited a stable change, while the Bio Ba value and Si/Ti ratio began to increase slightly, continuing until the end of the Younger Drays period (YD, 11.7–13.1 Cal ka BP). Overall, the levels of all three paleoproductivity proxies were higher during the Last Deglaciation than during the LGM, despite the low Si/Ti and Ca/Ti values at the end of the Last Deglaciation.

During the Holocene, the changes in all of the paleoproductivity proxies can be categorized into two distinct stages. In the Early and Middle Holocene, both the Bio Ba value and Si/Ti ratio began to

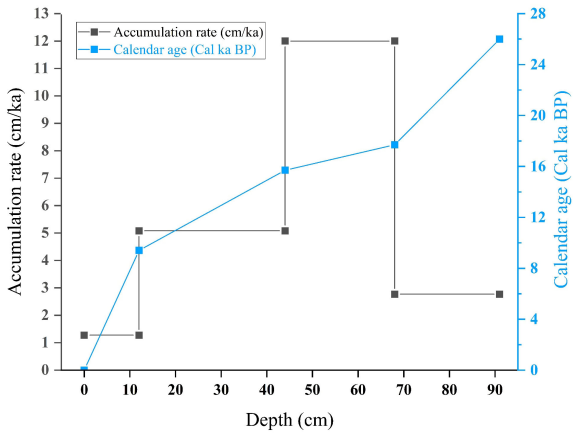

FIGURE 5
Accumulation rates and calibrated calendar ages for the top 91 cm of core ANT37-C5/6-07.

increase significantly and remained at high levels (Figures 2A, E), while the Ca/Ti ratio slowly decreased (Figure 2C). In the second stage (since the Middle Holocene, at ~6.6 Cal ka BP), the Bio Ba value and Si/Ti ratio underwent another slight increase. Although the Ca/Ti ratio remained at a relatively low level during the Late Holocene, it also exhibited an overall increasing trend.

4.3 Characteristics of the oxygenation proxies

As shown in Figure 2, the Mn/Ti ratio was relatively low during the LGM and began to increase during the Last Deglaciation. Similar to the paleoproductivity proxies, a significant peak occurred at ~15.8 Cal ka BP (Figure 2H). However, during the transition to the ACR, the increase in the Mn/Ti ratio became stagnant. Subsequently, from the YD period to the Holocene, the Mn/Ti ratio exhibited a rapid rebound, and the highest peak occurred at ~11.8 Cal ka BP. The change in the U content (XRF) was opposite to that of the Mn/Ti ratio (Figure 2I). It remained at a high value during the LGM. During the Last Deglaciation, it exhibited a continuous decreasing trend, and it remained at a low level during the Holocene. However, there is an absence of the large oxygenation peak in the U content (XRF) around 12 Cal ka BP. Our sampling point is located very close to the continental shelf, and the high Al and Ti contents at depths of 15-40 cm in the sediment core indicate a strong input of terrestrial material during this interval. This may have led to the significant deviation between the actual aU content and the total U content, which resulted in the absence of the peak point of U (XRF) curve.

5 Discussion

5.1 Source of the organic matter

Most regions of the Southern Ocean have a low primary productivity, which is typical of high nutrient and low chlorophyll oceans (Smith, 1991; Moore and Abbott, 2000; Gao and Chen, 2002). The total organic carbon (TOC) content within the upper 91 cm of core ANT37-C5/6-07 ranges from 0.10% to 0.63%, with an average value of 0.38%, which is close to those of other cores in the Cosmonaut Sea (Bonn, 1995; Yang et al., 2022). The downcore distribution pattern of the total nitrogen (TN) content is comparable to that of the TOC, with a strong positive correlation ($R^2 = 0.8687$) (Figure 6D). This indicates that the source of the organic matter in the core sediments was relatively stable, and the sources of the TOC and TN were consistent (Liu et al., 2014).

The ratio of the total organic carbon to the total nitrogen (TOC/TN) and the $\delta^{13}C$ content were used to determine whether the source of the organic matter in the marine sediments was terrestrial or oceanic (Prahl et al., 1994; Thornton and McManus, 1994; Meyers, 1997; Sampei and Matsumoto, 2001; Ogrinc et al., 2005). The TOC/TN ratio of organic matter derived from marine phytoplankton is typically 3–8, while that of organic matter from terrestrial sources is typically ≥20 (Emerson and Hedges, 1988; Gao et al., 2008). Marine organic carbon has a classic range of $\delta^{13}C$ value of −22 ‰ to −19 ‰ (Fontugne and Jouanneau, 1987), but previous studies have reported that the $\delta^{13}C$ value of the organic matter in Southern Ocean sediments tends to be more negative (Macko and Pereira, 1990; Harada et al., 1995; Domack et al., 1999; Domack et al., 2001; Kulbe et al., 2001; Berg et al., 2013; Han et al., 2015; Learman et al., 2016). This suggests that relying solely on the $\delta^{13}C$ values may not provide an accurate reference for the origin of the organic matter in Southern Ocean sediments. Therefore, in addition to the TOC/TN ratio and $\delta^{13}C$ value, we also utilized an end-component mixing model to estimate the proportions of the terrestrial and marine organic matter inputs (Eqs. (3)–(6)) (Mei et al., 2015):

$$TOC_{ter}(\%) = (\delta^{13}C_{mar} - \delta^{13}C_{sam})/(\delta^{13}C_{mar} - \delta^{13}C_{ter}) \times TOC_{sam}(\%) \quad (3)$$

$$TOC_{mar}(\%) = TOC_{sam}(\%) - TOC_{ter}(\%) \quad (4)$$

$$TOC_{mar-con}(\%) = TOC_{mar}(\%)/TOC_{sam}(\%) \times 100\% \quad (5)$$

$$TOC_{ter-con}(\%) = 1 - TOC_{mar-con}(\%) \quad (6)$$

where TOC_{ter} (%) and TOC_{mar} (%) are the percentages of terrestrial and oceanic organic carbon, respectively, $TOC_{ter\text{-}con}$ (%) and $TOC_{mar\text{-}con}$ (%) are the contributions of terrestrial and oceanic organic carbon, respectively, and TOC_{sam} (%) is the total organic carbon content of the sediment samples. $\delta^{13}C_{mar}$ is the $\delta^{13}C$ value of the sea-source organic matter endmember, which is the comprehensive level (−26.04‰) of the plankton, benthic organic matter, and seawater particulate organic matter in the Southern Ocean (Kopczyńska et al., 1995; Frazer, 1996; Gillies et al., 2012; Berg et al., 2013; Zhang et al., 2017). $\delta^{13}C_{ter}$ is the $\delta^{13}C$ value of the terrestrial organic matter endmember, which is taken from the cold vegetation on the Antarctic continent (−21.54‰) (Strauch et al., 2011). $\delta^{13}C_{sam}$ is the $\delta^{13}C$ value of the organic matter in the core sediments.

10.3389/fmars.2023.1215048

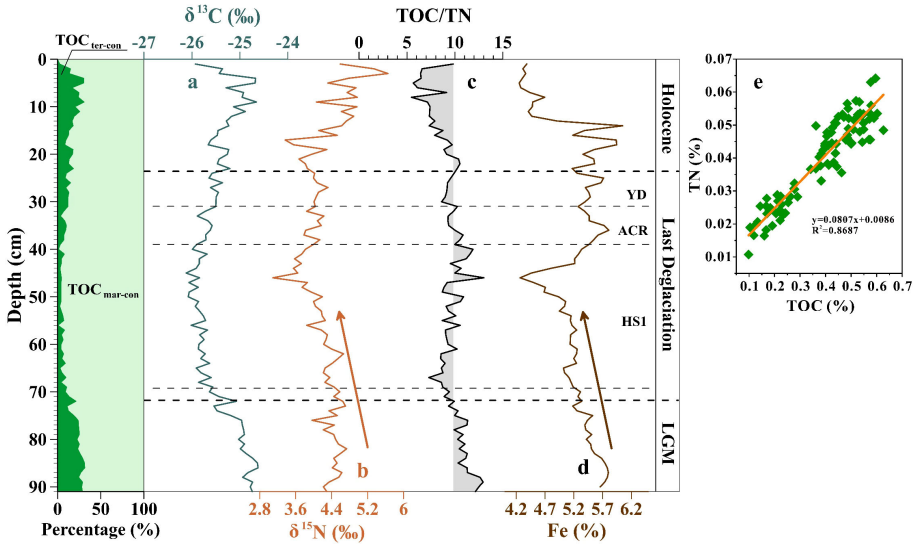

FIGURE 6
Downcore distribution patterns of the terrestrial and oceanic contribution ratios of the TOC, **(A)** δ13C, **(B)** δ15N, **(C)** TOC/TN ratios, **(D)** Fe content, and **(E)** the correlation between TOC (%) and TN (%).

According to the calculation results of the endmember mixing model (Table 2), the $TOC_{mar\text{-}con}$ (%) of the organic matter in the core sediments is 68.47%–99.46%, with an average value of 86.15%. Moreover, the TOC/TN ratio of the core organic matter is 5.48–13.01 (Figure 6C), with an average value of 9.51, which is very biased toward the TOC/TN ratio of marine organic matter (Thunell et al., 1992). Therefore, we believe that the vast majority of the organic matter came from marine export productivity, although the organic matter in core ANT37-C5/6-07 is interfered using the terrestrial input (Figure 6).

5.2 Changes in the paleoproductivity and the oxygenation

5.2.1 Last glacial maximum

The LGM occurred at approximately 19–26.5 Cal ka BP. During this period, the global temperature was relatively low, with an average temperature decrease of about 3–4°C. This period was characterized by the presence of massive continental ice sheets in both the Northern and Southern hemispheres (Adkins et al., 2002). In the seasonal sea ice regions surrounding the Antarctic continental margin, the main factors controlling the productivity are the lighting conditions, water ventilation, and sea ice cover (Anderson et al., 2002). During glacial to interglacial cycles, the sea ice cover fluctuates synchronously with the deep-ocean oxygen isotope records and Antarctic temperature, indirectly affecting the export production by regulating variables such as the lighting conditions, nutrient availability, and mixed layer depth (Dieckmann and Hellmer, 2003; Wolff et al., 2006; Bouttes et al., 2010; Abram et al., 2013). The sea salt Na^+ ($ssNa^+$) data from the EPICA DML (EDML) ice core serve as a proxy for sea ice expansion in the Indian Ocean sector of the Southern Ocean (Schüpbach et al., 2013). During the LGM, EDML-$ssNa^+$ content indicates that the Southern Ocean's sea ice coverage was extremely extensive (Figure 4D) (Fischer et al., 2007). The high abundance of *A. actinochilus* is also indicative of a cold environment and sea-ice expansion in the Cosmonaut Sea (Figure 4L) (Li et al., 2021). In the Antarctic coastal area, the >63 μm components of the marine sediments are typically deemed to be ice raft debris (IRD) (Diekmann and Kuhn, 1999; Liu et al., 2015; Lei et al., 2021). The IRD content reached a large peak during the early LGM (~25 Cal ka BP) (Figure 4H), signifying that sea ice expansion in the Cosmonaut Sea may have peaked during this period.

All the available proxies for core ANT37-C5/6-07 indicate that the paleoproductivity was extremely low during the LGM (Figures 4M–O), and the Bio Ba contents of cores PS1821-6 and PS1648-1 were also at a low value (Figures 4I, J) (Bonn, 1995). Even though the summer insolation in the Southern Hemisphere at 65°S was high (Figure 4C), the sea ice cover hindered the penetration of sunlight into the ocean and significantly reduced the amount of sunlight received by the

TABLE 2 Total organic carbon (TOC), percentages of terrestrial and oceanic organic carbon, and their contributions for the top 91 cm of core ANT37-C5/6-07.

	TOC (%)	TOC_{mar} (%)	TOC_{ter} (%)	$TOC_{mar\text{-}con}$ (%)	$TOC_{ter\text{-}con}$ (%)
Value range	0.10–0.63	0.07–0.57	0–0.18	68.47–99.46	0.54–31.53
Average value	0.38	0.33	0.05	86.15	13.85

surface ocean (Abram et al., 2013). The EDML-$\delta^{18}O$ content (Figure 4A) (EpicaCommunityMembers, 2006) also indicates the occurrence of low temperatures during the LGM, which severely limited the surface export productivity. However, the proportion of the Antarctic sea-ice algae in the phytoplankton in the surface ocean covered by sea ice may have increased during the LGM (Figure 4L). Ice algae, though usually not a significant contributor to the organic matter in benthic sediments, may have resulted in less negative $\delta^{13}C$ values during the LGM (Figure 6A) due to their relatively high $\delta^{13}C$ values (−15‰ to −8‰) (Gibson et al., 1999). The $\delta^{15}N$ value of sediment is often used to identify the nitrate bioavailability, and an increase in its value corresponds to an increase in the nutrient utilization by phytoplankton in the surface seawater (Francois et al., 1992; Altabet and Francois, 1994). The high $\delta^{15}N$ values during the LGM (Figure 6B) suggest that the nutrient utilization rate was relatively high despite the low paleoproductivity. However, the photosynthesis of phytoplankton should be hindered under thick sea ice coverage and lead to lower $\delta^{15}N$ values (Studer et al., 2015). This indicates that the nutrient supply may have been limited because of the weakened deep-water upwelling in the Cosmonaut Sea during this period (Kim et al., 2020), which is the major reason of the low export productivity at this time.

The Mn/Ti ratio was low during the LGM, while the U content (XRF) was high (Figures 4E, F), indicating significant depletion of oxygen due to pre-formed carbon storage and insufficient replenishment (Jaccard and Galbraith, 2012). The same evidence of the low oxygen content of the bottom water was obtained for the southwestern part of the Indian Ocean sector (Figure 4G) (Amsler et al., 2022). The radioactive ^{14}C ages indicate that poor ventilation conditions occurred in the deep sea during the LGM (Sarnthein et al., 2013; Skinner et al., 2017). The formation and activity of the sea ice in the Southern Ocean hindered gas exchange between the atmosphere and ocean and led to increased vertical stratification of the water column (Adkins et al., 2002; Watson and Naveira Garabato, 2006; Bouttes et al., 2010; Wolff et al., 2010; Adkins, 2013; Ferrari et al., 2014). Despite the fact that the solubility of oxygen increases at colder temperatures, it was difficult for the higher oxygen concentration surface water to reach the deeper layer to achieve refreshment and replenishment. Moreover, the bottom water (rich in nutrients) in the Cosmonaut Sea also failed to reach the surface ocean, which contributed to the extremely low export production. In summary, during the LGM, the paleoproductivity of the Cosmonaut Sea and the oxygenation level of the bottom water were primarily controlled by the constraints imposed by poor ventilation conditions.

Another impact of sea ice expansion was the northward movement of the upwelling zone in the Southern Ocean, which enhanced the sequestration of the respiratory carbon in the deep water along the coast of Antarctica, thereby reducing the amount of CO_2 emitted into the atmosphere (Toggweiler, 1999; Sigman and Boyle, 2000; Toggweiler et al., 2006; Watson et al., 2015). The biopump efficiency was found to be high during this period (Keir, 1988). In addition to the physical mechanisms, such as weakened ventilation and the northward movement of the upwelling zone, biogeochemical changes also played a positive role in the storage of carbon dioxide (François et al., 1997; Sigman and Boyle, 2000; Galbraith and Jaccard, 2015; Sigman et al., 2021). Due to the more comprehensive assimilation and utilization of nutrients (Figure 6B) and/or the relatively higher supply of iron containing terrestrial material (Figure 6D), more efficient biological carbon pumps were created in the Cosmonaut Sea during the LGM, further inhibiting the emission of CO_2 in the deep ocean (Studer et al., 2015; Gottschalk et al., 2016; Ai et al., 2020; Galbraith and Skinner, 2020).

5.2.2 Last deglaciation

It is widely believed that the Last Deglaciation began at 18–20 Cal ka BP, and the onset occurred later in East Antarctica than in West Antarctica (Fudge et al., 2013). The paleoproductivity proxy values in core ANT37-C5/6-07 began to increase significantly after 19.6 Cal ka BP (Figures 4N, O), and the oxygen content also exhibited a synchronous increase at this time (Figures 4E, F). Simultaneously, wind dust records from the EDML ice core also began to decrease from the peak. These data comprehensively indicate that the Last Deglaciation may have begun at ~19.6 Cal ka BP in the Southern Hemisphere (Jae Il et al., 2010; Yang et al., 2021).

The initial increase in the biogenic silicon content at the end of the last glacial period may have been due to the large consumption of siliceous nutrients in the water bodies south of the Antarctic Polar Front (Figure 4N) (Dumont et al., 2020). During HS1, the EDML-ssNa$^+$ value (Figure 4D), the IRD content (Figure 4H), and *A. actinochilus* abundance in core ANT36/C3-09 (Figure 4L) significantly decreased, indicating that the sea ice retreat process in the Cosmonaut Sea may have been approaching the end (Li et al., 2021). The sharp increases in Si/Ti and Ca/Ti ratios further suggest a rapid increase in the export productivity in the Cosmonaut Sea, which was likely due to significant amounts of nutrients and respiratory carbon reaching the surface ocean via the upwelling of deep water (Skinner et al., 2010; Jaccard et al., 2016; Gottschalk et al., 2020). With the decrease in the sea ice coverage, the surface layer of the Cosmonaut Sea received sufficient sunlight and the temperature increased in the Southern Hemisphere (Figure 4A), which may contribute to high levels of paleoproductivity (Frank et al., 2000; Kohfeld et al., 2005; Anderson et al., 2009; Jaccard et al., 2013; Thöle et al., 2019). In contrast, the $\delta^{15}N$ value continued to decline during HS1 and remained at a relatively low value (Figure 6B), indicating lower nutrient utilization compared to that during the LGM. This suggests that the decisive factor of increasing productivity was the increase in the nutrient supply from the lower layer of the Cosmonaut Sea, which also serves as evidence of enhanced ventilation (Kim et al., 2020). Macko and Estep (1984) argued that the oxidation of bottom water may lead to a decrease in bulk sedimentary $\delta^{15}N$ by suppressing the N isotope effect associated with denitrification (which generally produces low $\delta^{15}N$ NH_4^+). For instance, at ~12 Cal ka BP and ~16 Cal ka BP, two low values of $\delta^{15}N$ were observed in the core sediments, corresponding to the oxidation of bottom water during these two periods. However, empirical data, including the sediment trap results, suggest that even in slowly accumulating regions of the ocean, bulk sedimentary $\delta^{15}N$ records will primarily reflect changes in the $\delta^{15}N$ of exported N in most cases, rather than differential alteration (Robinson et al., 2012).

It should be noted that the Bio Ba values for core ANT37-C5/6-07 did not exhibit a significant peak during HS1 (Figure 4K), which is comparable with the data for cores PS1648-1 and PS1821-6 from the west of Cosmonaut Sea (Figures 4I, J) (Bonn, 1995). The preservation of biogenic barium is highly sensitive to changes in the paleoenvironmental conditions. When the sedimentary environment becomes oxygen or sulfate depleted, the solubility of $BaSO_4$ will greatly increase (McManus et al., 1998; Anderson et al., 2002; Beek et al., 2003; Tribovillard et al., 2006). McManus et al. (1998) argued that the Ba arriving at the seafloor under conditions of high carbon export and low bottom water oxygen may be poorly preserved—even in environments not showing significant porewater sulfate depletion. Poor preservation of Ba may also be indicated by high levels of aU. As shown in the Figure 7, during ~14–18 Cal ka BP, the Si/Ti ratios, U content (XRF), and TOC contents in the core sediments were relatively high, indicating the existence of such conditions of high organic carbon export and relatively low bottom-water oxygen, which led to the absence of a peak in the Bio Ba value during the middle stage of HS1.

An increase in the export productivity will lead to an increase in the consumption of oxygen via the decomposition of organic matter in the water body to some extent, causing a decrease in the oxygen content (Yamamoto et al., 2015). However, all of the records from the Cosmonaut Sea reveal that the oxygen content of the bottom water increased during this period (Figures 4E–G), indicating that the impact of organic matter remineralization on the oxygen content was minor (Amsler et al., 2022). To maintain oxygen levels, fresh and oxygen-rich surface seawater should be injected deep into the Cosmonaut Sea. We propose that the improved ventilation of the Southern Ocean during HS1, which was driven by the reduced generation of the North Atlantic Deep Water and the weakened Atlantic Meridional Overturning Circulation, played a major role in the increased oxygenation of the bottom water (McManus et al., 2004). The increase in water column temperature reduced the accumulation of respired carbon and possibly shifted the organic matter respiration to the upper water column, thereby decreasing the sinking flux of the organic matter to the abyss (Matsumoto, 2007). A deglacial decrease in the oceanic nutrient inventory could have also contributed to the reduction of the amount of organic matter available for respiration (Jaccard and Galbraith, 2012).

More importantly, it is crucial to note that the intensification of upwelling can result in an imbalance of the surface seawater's CO_2 budget. At the beginning of the last glacial termination period (TERM I) at ~17.5 Cal ka BP, radioactive carbon depleted CO_2 that was formed during the LGM and locked in the deep Southern Ocean was released into the atmosphere via the enhanced ventilation (Burke and Robinson, 2011; Bauska et al., 2016; Basak et al., 2018; Rae et al., 2018). Although the growth of phytoplankton was stimulated by the elevated nutrient levels, they were unable to completely assimilate and fix the dissolved carbon. This was evidenced by the low $\delta^{15}N$ values, indicating a low efficiency of the biological pump during this period, which permitted a considerable amount of CO_2 to escape into the atmosphere (Sigman et al., 2010; Studer et al., 2015).

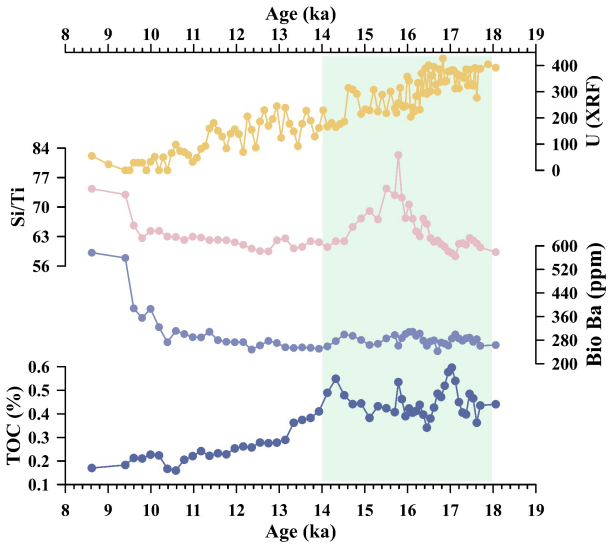

FIGURE 7
U content (XRF), Si/Ti ratios, Bio Ba content, and TOC content of core sediments during 8.6–18.1 Cal ka BP.

In the Southern Hemisphere, there was a cold period, which interrupted the warming trend near the deglacial midpoint, i.e., the ACR (14.7–13.1 Cal ka BP) (Shakun et al., 2012). The EDML-ssNa$^+$ value and *A. actinochilus* abundance rebounded during the ACR (Figures 4D, L), indicating that the sea ice resumed activity. The decrease in the summer insolation at 65°S (Figure 4C), coupled with the reflection from the sea ice and the temperature regulation (Figures 4A, K), limited the surface productivity of the Southern Ocean. The decrease in the productivity output also means that the nutrient supplementation in the surface seawater was deficient during the ACR, which may have been associated with the weakening of upwelling (Jaccard et al., 2013). This corresponded to a temporary cessation of the increase in the atmospheric CO_2 content (Figure 4B). The changes in the Mn/Ti ratio and U content (XRF) in core ANT37-C5/6-07 and the aU content in core PS2603-3 stagnated during the ACR (Figures 4E–G), indicating that the supplementation of the oxygen content in the deep Cosmonaut Sea was interrupted, which is further proof of the weakened ventilation in the study area.

During the YD, there was a notable improvement in the oxygenation levels of the bottom water in the Cosmonaut Sea (Figures 4E, F), but the improvement of the export productivity was very minimal (Figures 4M–O). The efficiency of the biological pump remained consistent with that during the ACR, i.e., it remained at a low level. The atmospheric CO_2 content continued to rise as it was supplemented by deep sea respiratory carbon (Figure 4B). In conclusion, during the HS1 period, the booming productivity of the Cosmonaut Sea was attributed to the favorable sunlight conditions and the increase in the nutrient supply by the enhanced ventilation, the latter also greatly facilitated the gas exchange between the surface and deep waters. However, during the latter half of the Last Deglaciation, the decrease in sunlight

intensity in the high-latitude regions of the Southern Hemisphere dominated the surface productivity of the Cosmonaut Sea.

5.2.3 Holocene

During the Early Holocene, the records in core ANT37-C5/6-07 indicate that a significant increase in siliceous productivity occurred (Figures 4M, N). However, the Ca/Ti ratio, which had previously been consistent with the Si/Ti ratio, exhibited a decreasing trend. The oxygen concentration of the bottom water remained high during the Early and Middle Holocene. Since the Middle Holocene (~5.5 Cal ka BP), the paleoproductivity in the Cosmonaut Sea has been comprehensively improved and maintained at a high level. The Bio Ba patterns of cores PS1648-1 and PS1821-6 are similar to that of core ANT37-C5/6-07 (Figures 4I, J, M). This suggests that the change in paleoproductivity may have been a more widespread phenomenon in the Indian Ocean sector of the Southern Ocean, rather than a regional characteristic.

We found that changes in the paleoproductivity were consistent with the variations in the summer solar radiation at 65°S in the Southern Hemisphere (Figure 4C), which helps to explain the widespread conditions mentioned above. During the Holocene, the amount of summer insolation in the high-latitude region in the Southern Hemisphere increased significantly. The retreat of the sea ice led to a reduction in the sunlight blocking efficiency, thus prolonging surface water exposure, which may have been one of the causes of the significant increase in the productivity in the Cosmonaut Sea since ~ 9.4 Cal ka BP (Boyd et al., 2001; Denis et al., 2010; Cheah et al., 2013). Furthermore, the utilization rate of nutrients indicated by the $\delta^{15}N$ values in the core reached a high level (Figure 6B), which was decoupled from Fe availability (Figure 6D) and was closely linked to the rapid increase in surface productivity during this time period. The existence of a tightly coupled glacier-sea ice-ocean system driven by insolation changes throughout the Holocene has also been revealed by the sedimentary records of the Adélie Land in the East Antarctica (Crosta et al., 2008; Denis et al., 2009a; Denis et al., 2009b; Denis et al., 2010). The high oxygen content of the bottom water of the Cosmonaut Sea suggests that deep-water ventilation has been favorable during the Holocene. Despite the negative effects of both the high export productivity (Figures 4M, N) and the increase in temperature (Figure 4K), the enhanced ventilation dominated the level of oxygenation, leading to the overall high oxygen content of the Cosmonaut Sea bottom water during the Holocene.

The East Cosmonaut Sea Polynya (ECP) may be another important driving factor of the local paleoproductivity and oxygenation changes. Comiso and Gordon (1996) reported that the ECP occurs regularly on a long-term basis, with an average central position at 65°S (range of 64–66°S) and 52°E (range of 42–57°E) near Cape Ann during winter in the Southern Hemisphere. This polynya is among the most persistent polynyas in the Southern Ocean, and it has been observed almost every year since the availability of satellite passive microwave data in December 1972. The formation of the ECP may have been triggered by either ocean forcing (Comiso and Gordon, 1996) or offshore divergent winds (Arbetter et al., 2004; Bailey et al., 2004) or a combination of both processes (Figure 7) (Prasad et al., 2005). The unique configuration of the coastline plays an important role in this process (Comiso and Gordon, 1996; Prasad et al., 2005). Due to the vast northward extension of Cape Ann, the westward flowing CC and the eastward flowing ACC form a high level of boundary forcing in this region. According to climatological data, it has been argued that this offshore location experienced upwelling of the warm salty CDW, which broke the original sea ice cover, and may have also played a key role in promoting deep-sea ventilation (Figure 8) (Prasad et al., 2005). The newly formed sea ice is constantly pushed off the coast by strong katabatic winds (Francis et al., 2019). The increase in the IRD content in the core sediments since ~9.4 Cal ka BP was likely caused by the continuous offshore transportation, dissolution, and release of detrital materials carried by fragmented sea ice (Figure 4H).

A previous study has shown that the chlorophyll-*a* concentration is higher in the Maud Rise Polynya than in the surrounding region during austral spring (von Berg et al., 2020). Jena and Pillai (2020) suggested that this could be the result of the improved irradiance conditions and increased iron supply through upwelling after the formation of polynyas. During the Holocene, the sea surface temperature of the Cosmonaut Sea was higher than during the Last Glacial Maximum, and there was a decrease in the abundance of *A. actinochilus* (Figures 4K, L), which indicates a decrease in sea ice concentration during this period. Based on the positive impact of the polynya system on the local export productivity and deep-water ventilation, combined with the increase in the IRD content of the benthic sediments, we speculate that the formation and development history of the ECP can be traced back to ~9.4 Cal ka BP, but we still lack more evidence of changes in ECP on the millennial scale. In general, the Cosmonaut Sea region was in a well-ventilated state during the Holocene.

6 Conclusions

Valuable proxies reveal that the paleoproductivity and oxygen levels were low in the Cosmonaut Sea during the LGM. Furthermore, the nutrient utilization rate by the phytoplankton in the surface seawater was at a relatively high level. This indicates that the Cosmonaut Sea deep water was in a state of weak ventilation, which hindered the nutrient supply to the surface ocean. The pre-formed carbon storage led to significant oxygen consumption, while the respiratory CO_2 formed was trapped in the deep Southern Ocean. This likely contributed to the low atmospheric CO_2 content during the LGM period.

During the Last Deglaciation, a significant increase in the export productivity was caused by the increase in the nutrient supply from the deep Cosmonaut Sea. However, the utilization rate of nutrients was low, indicating the inefficient assimilation of nutrients and dissolved CO_2 by the phytoplankton in the surface seawater. A large amount of respiratory CO_2 was released into the atmosphere via the enhanced ventilation. In addition, the supplementation of the dissolved oxygen from the surface water exceeded the consumption caused by the increased export productivity, leading to an improvement in the degree of oxygenation. However, there were noticeable interruptions

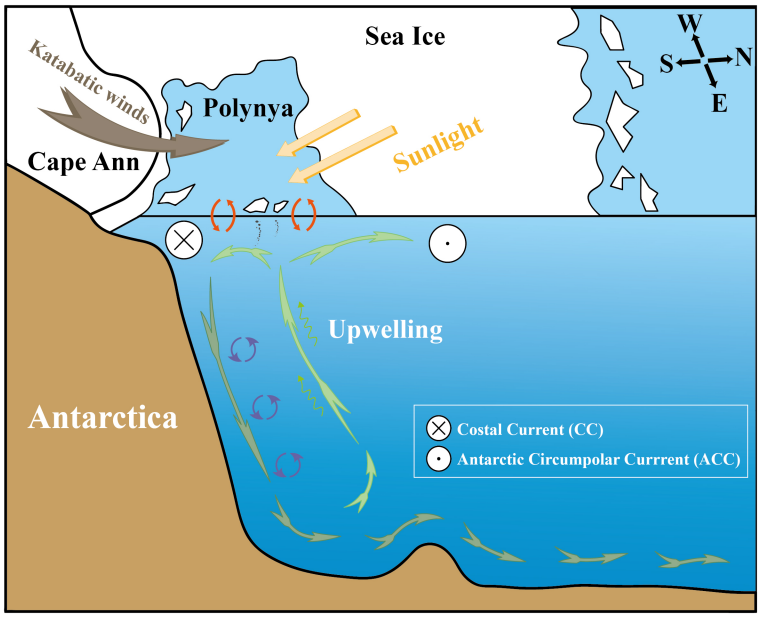

FIGURE 8
Enhanced ventilation under the East Cosmonaut Polynya conditions since the Holocene.

during the Last Deglaciation, which were triggered by the transitions from the HS1 to the ACR.

The paleoproductivity in the Cosmonaut Sea experienced two increases in the Early Holocene and Middle Holocene respectively. We speculate that the changes in the summer insolation at high southern latitudes have significantly contributed to the increased productivity. After the Middle Holocene, there was a comprehensive improvement in the productivity within the Indian Ocean sector of the Southern Ocean, accompanied by a simultaneous increase in the nutrient utilization rates. The replenishment of oxygen dominated the changes in the oxygen content of the bottom-water, which was potentially related to the enhanced ventilation during the Holocene and/or the formation of the East Cosmonaut Sea Polynya.

Data availability statement

The raw data supporting the conclusions of this article will be made available by the authors, without undue reservation.

Author contributions

The contribution from the authors are as follows: LH: methodology, data analysis and visualization, paper writing. YZ: conceptualization of the study and data acquisition. YW: methodology, data acquisition and data curation. PM: data analysis and data visualization. WW: methodology and data curation. QG: core chronology methodology, funding acquisition. YB: methodology, data curation and paper revision. XH: investigation, methodology, paper revision and funding acquisition. All authors contributed to the article and approved the submitted version

Funding

This research is funded by National Key R&D Program of China (2022YFC2905500), Impact and Response of Antarctic Seas to Climate Change (IRASCC2020-2022).

Acknowledgments

We are very grateful to all of the scientific expedition staff, especially the teachers and students of the Marine Geology and the Geophysics Working Group, and all of the crew of the R/V "XUELONG2" icebreaker for their hard work in sampling during the 37th Chinese Antarctic Research Expedition. We sincerely thank the Chinese Arctic and Antarctic Administration and Polar Research Institute of China for their great help in this research.

Conflict of interest

The authors declare that the research was conducted in the absence of any commercial or financial relationships that could be construed as a potential conflict of interest.

Publisher's note

All claims expressed in this article are solely those of the authors and do not necessarily represent those of their affiliated organizations, or those of the publisher, the editors and the reviewers. Any product that may be evaluated in this article, or claim that may be made by its manufacturer, is not guaranteed or endorsed by the publisher.

References

Abram, N. J., Wolff, E. W., and Curran, M. A. J. (2013). A review of sea ice proxy information from polar ice cores. *Quat. Sci. Rev.* 79, 168–183. doi: 10.1016/j.quascirev.2013.01.011

Adkins, J. F. (2013). The role of deep ocean circulation in setting glacial climates. *Paleoceanography* 28 (3), 539–561. doi: 10.1002/palo.20046

Adkins, J. F., McIntyre, K., and Schrag, D. P. (2002). The salinity, temperature, and $\delta^{18}O$ of the glacial deep ocean. *Science* 298 (5599), 1769–1773. doi: 10.1126/science.1076252

Agnihotri, R., Altabet, M. A., Herbert, T. D., and Tierney, J. E. (2008). Subdecadally resolved paleoceanography of the Peru margin during the last two millennia. *Geochem. Geophys. Geosystems* 9 (5), Q05013. doi: 10.1029/2007GC001744

Ai, X. E., Studer, A. S., Sigman, D. M., Martínez-García, A., Fripiat, F., Thöle, L. M., et al. (2020). Southern Ocean upwelling, Earth's obliquity, and glacial-interglacial atmospheric CO_2 change. *Science* 370 (6522), 1348–1352. doi: 10.1126/science.abd2115

Altabet, M. A., and Francois, R. (1994). Sedimentary nitrogen isotopic ratio as a recorder for surface ocean nitrate utilization. *Glob. Biogeochem. Cycles* 8 (1), 103–116. doi: 10.1029/93GB03396

Amsler, H. E., Thöle, L. M., Stimac, I., Geibert, W., Ikehara, M., Kuhn, G., et al. (2022). Bottom water oxygenation changes in the Southwestern Indian Ocean as an indicator for enhanced respired carbon storage since the last glacial inception. *Climate Past* 18 (8), 1797–1813. doi: 10.5194/cp-18-1797-2022

Anderson, R. F., Ali, S., Bradtmiller, L. I., Nielsen, S. H. H., Fleisher, M. Q., Anderson, B. E., et al. (2009). Wind-driven upwelling in the southern ocean and the deglacial rise in atmospheric CO_2. *Science* 323 (5920), 1443–1448. doi: 10.1126/science.1167441

Anderson, R. F., Chase, Z., Fleisher, M. Q., and Sachs, J. (2002). The Southern Ocean's biological pump during the Last Glacial Maximum. *Deep Sea Res. Part II: Topical Stud. Oceanography* 49 (9), 1909–1938. doi: 10.1016/S0967-0645(02)00018-8

Anderson, R. F., Sachs, J. P., Fleisher, M. Q., Allen, K. A., Yu, J., Koutavas, A., et al. (2019). Deep-sea oxygen depletion and ocean carbon sequestration during the last ice age. *Glob. Biogeochem. Cycles* 33 (3), 301–317. doi: 10.1029/2018GB006049

Andrews, J. T., Domack, E. W., Cunningham, W. L., Leventer, A., Licht, K. J., Jull, A. J. T., et al. (1999). Problems and possible solutions concerning radiocarbon dating of surface marine sediments, ross sea, Antarctica. *Quat. Res.* 52 (2), 206–216. doi: 10.1006/qres.1999.2047

Anilkumar, N., Chacko, R., Sabu, P., Pillai, H. U. K., George, J. V., and Achuthankutty, C. T. (2014). Biological response to physical processes in the Indian Ocean sector of the Southern Ocean: a case study in the coastal and oceanic waters. *Environ. Monit. Assess.* 186 (12), 8109–8124. doi: 10.1007/s10661-014-3990-4

Aoki, S., Katsumata, K., Hamaguchi, M., Noda, A., Kitade, Y., Shimada, K., et al. (2020). Freshening of antarctic bottom water off cape darnley, East Antarctica. *J. Geophysical Research: Oceans* 125 (8), e2020JC016374. doi: 10.1029/2020JC016374

Arbetter, T. E., Lynch, A. H., and Bailey, D. A. (2004). Relationship between synoptic forcing and polynya formation in the Cosmonaut Sea: 1. Polynya climatology. *J. Geophysical Research: Oceans* 109 (C4), C04022. doi: 10.1029/2003JC001837

Armand, L. K., Crosta, X., Romero, O., and Pichon, J.-J. (2005). The biogeography of major diatom taxa in Southern Ocean sediments: 1. Sea ice related species. *Palaeogeogr. Palaeoclimatol. Palaeoecol.* 223 (1), 93–126. doi: 10.1016/j.palaeo.2005.02.015

Bailey, D. A., Lynch, A. H., and Arbetter, T. E. (2004). Relationship between synoptic forcing and polynya formation in the Cosmonaut Sea: 2. Regional climate model simulations. *J. Geophysical Research: Oceans* 109 (C4), C04022. doi: 10.1029/2003JC001838

Basak, C., Fröllje, H., Lamy, F., Gersonde, R., Benz, V., Anderson, R., et al. (2018). Breakup of last glacial deep stratification in the South Pacific. *Science* 359, 900–904. doi: 10.1126/science.aao2473

Bauska, T. K., Baggenstos, D., Brook, E. J., Mix, A. C., Marcott, S. A., Petrenko, V. V., et al. (2016). Carbon isotopes characterize rapid changes in atmospheric carbon dioxide during the last deglaciation. *Proc. Natl. Acad. Sci. U.S.A.* 113 (13), 3465–3470. doi: 10.1073/pnas.1513868113

Beek, P., Reyss, J.-L., Bonté, P., and Schmidt, S. (2003). Sr/Ba in barite: A proxy of barite preservation in marine sediments? *Mar. Geol.* 199, 205–220. doi: 10.1016/S0025-3227(03)00220-2

Berg, S., Leng, M. J., Kendrick, C. P., Cremer, H., and Wagner, B. (2013). Bulk sediment and diatom silica carbon isotope composition from coastal marine sediments off East Antarctica. *Silicon* 5 (1), 19–34. doi: 10.1007/s12633-012-9113-3

Bibik, V. A., Maslennikov, V. V., Pelevin, A. S., Polonsky, V. E., and Solyankin, E. V. (1988). "The current system and the distribution of waters of different modifications in the Cosmonaut Sea," in *Interdisciplinary investigations of pelagic ecosystem in the commonwealth and cosmonaut seas*. Eds. T. G. Lubimova, R. R. Makarov, V. V. Maslennikov, E. Z. Samyshev, V. A. Bibik and T. G. Tarverdieva (Moscow: VNIRO Publishers), 16–43.

Bonn, W. J. (1995). "Biogenopal und biogenes Barium als Indikatoren für spätquartäre Produktivitätsänderungen am antarktischen Kontinentalhang, atlantischer Sektor (Biogenic opal and barium: Indicators for late Quarternary changes in productivity at the Antarctic continental margin, Atlantic Sector)," in *Berichte zur polarforschung = Reports on polar research* (Bremerhaven, Germany: Alfred-Wegener-Institut für Polar- und Meeresforschung), 1–186.

Bonn, W. J., Gingele, F. X., Grobe, H., Mackensen, A., and Fütterer, D. K. (1998). Palaeoproductivity at the Antarctic continental margin: Opal and barium records for the last 400 ka. *Palaeogeogr. Palaeoclimatol. Palaeoecol.* 139 (3), 195–211. doi: 10.1016/S0031-0182(97)00144-2

Bouttes, N., Paillard, D., and Roche, D. M. (2010). Impact of brine-induced stratification on the glacial carbon cycle. *Clim. Past* 6 (5), 575–589. doi: 10.5194/cp-6-575-2010

Boyd, P. W., Crossley, A. C., DiTullio, G. R., Griffiths, F. B., Hutchins, D. A., Queguiner, B., et al. (2001). Control of phytoplankton growth by iron supply and irradiance in the subantarctic Southern Ocean: Experimental results from the SAZ Project. *J. Geophysical Research: Oceans* 106 (C12), 31573–31583. doi: 10.1029/2000JC000348

Brown, E. T., Le Callonnec, L., and German, C. R. (2000). Geochemical cycling of redox-sensitive metals in sediments from lake Malawi: A diagnostic paleotracer for episodic changes in mixing depth. *Geochimica Cosmochimica Acta* 64 (20), 3515–3523. doi: 10.1016/S0016-7037(00)00460-9

Brumsack, H. J. (1989). Geochemistry of recent TOC-rich sediments from the Gulf of California and the Black Sea. *Geologische Rundschau* 78 (3), 851–882. doi: 10.1007/BF01829327

Burke, A., and Robinson, L. (2011). The Southern ocean's role in carbon exchange during the last deglaciation. *Sci. (New York N.Y.)* 335, 557–561. doi: 10.1126/science.1208163

Calvert, S. E., and Pedersen, T. F. (1993). Geochemistry of Recent oxic and anoxic marine sediments: Implications for the geological record. *Mar. Geol.* 113 (1), 67–88. doi: 10.1016/0025-3227(93)90150-T

Calvert, S. E., and Pedersen, T. F. (1996). Sedimentary geochemistry of manganese; implications for the environment of formation of manganiferous black shales. *Econ. Geol.* 91 (1), 36–47. doi: 10.2113/gsecongeo.91.1.36

Cheah, W., McMinn, A., Griffiths, F. B., Westwood, K. J., Wright, S. W., and Clementson, L. A. (2013). Response of phytoplankton photophysiology to varying environmental conditions in the sub-antarctic and polar frontal zone. *PLoS One* 8 (8), e72165. doi: 10.1371/journal.pone.0072165

Cheshire, H., and Thurow, J. W. (2005). Late Quaternary climate change record from two long sediment cores from Guaymas Basin, Gulf of California. *J. Quat. Sci.* 20 (5), 457–469. doi: 10.1002/jqs.944

Comiso, J. C. (2003). "Large-scale characteristics and variability of the global sea ice cover," in *Sea ice*. (Oxford: Blackwell), 112–142.

Comiso, J. C., and Gordon, A. L. (1996). Cosmonaut polynya in the Southern Ocean: Structure and variability. *J. Geophysical Research: Oceans* 101 (C8), 18297–18313. doi: 10.1029/96JC01500

Crosta, X., Denis, D., and Ther, O. (2008). Sea ice seasonality during the Holocene, Adélie Land, East Antarctica. *Mar. Micropaleontol.* 66 (3), 222–232. doi: 10.1016/j.marmicro.2007.10.001

Crosta, X., Romero, O., Armand, L. K., and Pichon, J.-J. (2005). The biogeography of major diatom taxa in Southern Ocean sediments: 2. Open ocean related species. *Palaeogeogr. Palaeoclimatol. Palaeoecol.* 223 (1), 66–92. doi: 10.1016/j.palaeo.2005.03.028

Dehairs, F., Chesselet, R., and Jedwab, J. (1980). Discrete suspended particles of barite and the barium cycle in the open ocean. *Earth Planetary Sci. Lett.* 49 (2), 528–550. doi: 10.1016/0012-821X(80)90094-1

Dehairs, F., Stroobants, N., and Goeyens, L. (1991). Suspended barite as a tracer of biological activity in the Southern Ocean. *Mar. Chem.* 35 (1), 399–410. doi: 10.1016/S0304-4203(09)90032-9

DeMaster, D. J., Nelson, T. M., Harden, S. L., and Nittrouer, C. A. (1991). The cycling and accumulation of biogenic silica and organic carbon in Antarctic deep-sea and continental margin environments. *Mar. Chem.* 35 (1), 489–502. doi: 10.1016/S0304-4203(09)90039-1

Denis, D., Crosta, X., Barbara, L., Massé, G., Renssen, H., Ther, O., et al. (2010). Sea ice and wind variability during the Holocene in East Antarctica: Insight on middle-high latitude coupling. *Quat. Sci. Rev.* 29 (27), 3709–3719. doi: 10.1016/j.quascirev.2010.08.007

Denis, D., Crosta, X., Schmidt, S., Carson, D. S., Ganeshram, R. S., Renssen, H., et al. (2009a). Holocene glacier and deep water dynamics, Adélie Land region, East Antarctica. *Quat. Sci. Rev.* 28 (13), 1291–1303. doi: 10.1016/j.quascirev.2008.12.024

Denis, D., Crosta, X., Schmidt, S., Carson, D. S., Ganeshram, R. S., Renssen, H., et al. (2009b). Holocene productivity changes off Adélie Land (East Antarctica). *Paleoceanography* 24 (3), PA3207. doi: 10.1029/2008PA001689

Dieckmann, G. S., and Hellmer, H. H. (2003). "The importance of sea ice: An overview," in *Sea ice*. (Oxford: Blackwell), 1–21.

Diekmann, B., and Kuhn, G. (1999). Provenance and dispersal of glacial–marine surface sediments in the Weddell Sea and adjoining areas, Antarctica: Ice-rafting versus current transport. *Mar. Geol.* 158 (1), 209–231. doi: 10.1016/S0025-3227(98)00165-0

Domack, E. W., Jacobson, E. A., Shipp, S., and Anderson, J. B. (1999). Late Pleistocene–Holocene retreat of the West Antarctic Ice-Sheet system in the Ross Sea:

Part 2—Sedimentologic and stratigraphic signature. *GSA Bull.* 111 (10), 1517–1536. doi: 10.1130/0016-7606(1999)111<1517:LPHROT>2.3.CO;2

Domack, E., Leventer, A., Dunbar, R., Taylor, F., Brachfeld, S., and Sjunneskog, C. (2001). Chronology of the Palmer Deep site, Antarctic Peninsula: a Holocene palaeoenvironmental reference for the circum-Antarctic. *Holocene* 11 (1), 1–9. doi: 10.1191/095968301673881493

Dumont, M., Pichevin, L., Geibert, W., Crosta, X., Michel, E., Moreton, S., et al. (2020). The nature of deep overturning and reconfigurations of the silicon cycle across the last deglaciation. *Nat. Commun.* 11 (1), 1534. doi: 10.1038/s41467-020-15101-6

Durgadoo, J. V., Lutjeharms, J. R. E., Biastoch, A., and Ansorge, I. J. (2008). The conrad rise as an obstruction to the antarctic circumpolar current. *Geophysical Res. Lett.* 35 (20), L20606. doi: 10.1029/2008GL035382

Dymond, J., Suess, E., and Lyle, M. (1992). Barium in deep-sea sediment: A geochemical proxy for paleoproductivity. *Paleoceanography* 7 (2), 163–181. doi: 10.1029/92PA00181

Emerson, S., and Hedges, J. I. (1988). Processes controlling the organic carbon content of open ocean sediments. *Paleoceanography* 3 (5), 621–634. doi: 10.1029/PA003i005p00621

EpicaCommunityMembers (2006). One-to-one coupling of glacial climate variability in Greenland and Antarctica. *Nature* 444 (7116), 195–198. doi: 10.1038/nature05301

Esper, O., and Gersonde, R. (2014a). New tools for the reconstruction of Pleistocene Antarctic sea ice. *Palaeogeogr. Palaeoclimatol. Palaeoecol.* 399, 260–283. doi: 10.1016/j.palaeo.2014.01.019

Esper, O., and Gersonde, R. (2014b). Quaternary surface water temperature estimations: New diatom transfer functions for the Southern Ocean. *Palaeogeogr. Palaeoclimatol. Palaeoecol.* 414, 1–19. doi: 10.1016/j.palaeo.2014.08.008

Esper, O., Gersonde, R., and Kadagies, N. (2010). Diatom distribution in southeastern Pacific surface sediments and their relationship to modern environmental variables. *Palaeogeogr. Palaeoclimatol. Palaeoecol.* 287 (1), 1–27. doi: 10.1016/j.palaeo.2009.12.006

Fagel, N., Dehairs, F., André, L., Bareille, G., and Monnin, C. (2002). Ba distribution in surface Southern Ocean sediments and export production estimates. *Paleoceanography* 17 (2), 1–1-1-20. doi: 10.1029/2000PA000552

Ferrari, R., Jansen, M. F., Adkins, J. F., Burke, A., Stewart, A. L., and Thompson, A. F. (2014). Antarctic sea ice control on ocean circulation in present and glacial climates. *Proc. Natl. Acad. Sci.* 111 (24), 8753–8758. doi: 10.1073/pnas.1323922111

Fischer, H., Fundel, F., Ruth, U., Twarloh, B., Wegner, A., Udisti, R., et al. (2007). Reconstruction of millennial changes in dust emission, transport and regional sea ice coverage using the deep EPICA ice cores from the Atlantic and Indian Ocean sector of Antarctica. *Earth Planetary Sci. Lett.* 260 (1), 340–354. doi: 10.1016/j.epsl.2007.06.014

Fontugne, M. R., and Jouanneau, J.-M. (1987). Modulation of the particulate organic carbon flux to the ocean by a macrotidal estuary: Evidence from measurements of carbon isotopes in organic matter from the Gironde system. *Estuarine Coast. Shelf Sci.* 24 (3), 377–387. doi: 10.1016/0272-7714(87)90057-6

Francis, D., Eayrs, C., Cuesta, J., and Holland, D. (2019). Polar cyclones at the origin of the reoccurrence of the maud rise polynya in austral winter 2017. *J. Geophysical Research: Atmospheres* 124 (10), 5251–5267. doi: 10.1029/2019JD030618

Francois, R., Altabet, M. A., and Burckle, L. H. (1992). Glacial to interglacial changes in surface nitrate utilization in the Indian Sector of the Southern Ocean as recorded by sediment δ^{15}N. *Paleoceanography* 7 (5), 589–606. doi: 10.1029/92PA01573

François, R., Altabet, M. A., Yu, E.-F., Sigman, D. M., Bacon, M. P., Frank, M., et al. (1997). Contribution of Southern Ocean surface-water stratification to low atmospheric CO_2 concentrations during the last glacial period. *Nature* 389 (6654), 929–935. doi: 10.1038/40073

Frank, M., Gersonde, R., van der Loeff, M. R., Bohrmann, G., Nürnberg, C. C., Kubik, P. W., et al. (2000). Similar glacial and interglacial export bioproductivity in the Atlantic Sector of the Southern Ocean: Multiproxy evidence and implications for glacial atmospheric CO_2. *Paleoceanography* 15 (6), 642–658. doi: 10.1029/2000PA000497

Frazer, T. K. (1996). Stable isotope composition (δ^{13}C and δ^{15}N) of larval krill, Euphausia superba, and two of its potential food sources in winter. *J. Plankton Res.* 18 (8), 1413–1426. doi: 10.1093/plankt/18.8.1413

Fudge, T. J., Steig, E. J., Markle, B. R., Schoenemann, S. W., Ding, Q., Taylor, K. C., et al. (2013). Onset of deglacial warming in West Antarctica driven by local orbital forcing. *Nature* 500 (7463), 440–444. doi: 10.1038/nature12376

Galbraith, E. D., and Jaccard, S. L. (2015). Deglacial weakening of the oceanic soft tissue pump: global constraints from sedimentary nitrogen isotopes and oxygenation proxies. *Quat. Sci. Rev.* 109, 38–48. doi: 10.1016/j.quascirev.2014.11.012

Galbraith, E. D., and Skinner, L. C. (2020). The biological pump during the last glacial maximum. *Ann. Rev. Mar. Sci.* 12, 559–586. doi: 10.1146/annurev-marine-010419-010906

Gao, Z.-Y., and Chen, L.-Q. (2002). Study of carbon cycling in the southern ocean: A review. *World Sci-Tech R D* 04), 41–48. doi: 10.16507/j.issn.1006-6055.2002.04.012

Gao, X.-L., Chen, S.-Y., Ma, F.-J., Dang, A.-C., and Long, A.-M. (2008). Distribution and source characteristics of carbon and nitrogen and their burial fluxes in two core sediments from western Nansha Islands sea area. *J. Trop. Oceanography* 27 (03), 38–44.

Gao, Z.-Y., Chen, L.-Q., and Wang, W.-Q. (2001). Air-sea fluxes and the distribution of sink and source of CO2 between 80°W and 80°E in the Southern Ocean. *Chin. J. Polar Res.* 13 (3), 263–269.

Gersonde, R., Crosta, X., Abelmann, A., and Armand, L. (2005). Sea-surface temperature and sea ice distribution of the Southern Ocean at the EPILOG Last Glacial Maximum—a circum-Antarctic view based on siliceous microfossil records. *Quat. Sci. Rev.* 24 (7), 869–896. doi: 10.1016/j.quascirev.2004.07.015

Gibson, J. A. E., Trull, T., Nichols, P. D., Summons, R. E., and McMinn, A. (1999). Sedimentation of ^{13}C-rich organic matter from Antarctic sea-ice algae: A potential indicator of past sea-ice extent. *Geology* 27 (4), 331–334. doi: 10.1130/0091-7613(1999)027<0331:SOCROM>2.3.CO;2

Gillies, C. L., Stark, J. S., and Smith, S. D. A. (2012). Research article: small-scale spatial variation of δ^{13}C and δ^{15}N isotopes in Antarctic carbon sources and consumers. *Polar Biol.* 35 (6), 813–827. doi: 10.1007/s00300-011-1126-7

Gingele, F., and Dahmke, A. (1994). Discrete barite particles and barium as tracers of paleoproductivity in south Atlantic sediments. *Paleoceanography* 9 (1), 151–168. doi: 10.1029/93PA02559

Gottschalk, J., Michel, E., Thöle, L. M., Studer, A. S., Hasenfratz, A. P., Schmid, N., et al. (2020). Glacial heterogeneity in Southern Ocean carbon storage abated by fast South Indian deglacial carbon release. *Nat. Commun.* 11 (1), 6192. doi: 10.1038/s41467-020-20034-1

Gottschalk, J., Skinner, L. C., Lippold, J., Vogel, H., Frank, N., Jaccard, S. L., et al. (2016). Biological and physical controls in the Southern Ocean on past millennial-scale atmospheric CO_2 changes. *Nat. Commun.* 7 (1), 11539. doi: 10.1038/ncomms11539

Graham, R. M., De Boer, A. M., van Sebille, E., Kohfeld, K. E., and Schlosser, C. (2015). Inferring source regions and supply mechanisms of iron in the Southern Ocean from satellite chlorophyll data. *Deep Sea Res. Part I: Oceanographic Res. Papers* 104, 9–25. doi: 10.1016/j.dsr.2015.05.007

Han, X.-B., Zhao, J., Chu, F.-Y., Pan, J.-M., Tang, L.-G., Xu, D., et al. (2015). The source of organic matter and its sedimentary environment of the bottom surface sediment in northeast waters to Antarctic Peninsula based on the biomarker features. *Haiyang Xuebao* 37 (8), 26–38. doi: 10.3969/j.issn.0253-4193.2015.08.003

Harada, N., Handa, N., Fukuchi, M., and Ishiwatari, R. (1995). Source of hydrocarbons in marine sediments in Lützow-Holm Bay, Antarctica. *Org. Geochem.* 23 (3), 229–237. doi: 10.1016/0146-6380(94)00124-J

Heaton, T. J., Köhler, P., Butzin, M., Bard, E., Reimer, R. W., Austin, W. E. N., et al. (2020). Marine20—The marine radiocarbon age calibration curve (0–55,000 cal BP). *Radiocarbon* 62 (4), 779–820. doi: 10.1017/RDC.2020.68

Heywood, K. J., Sparrow, M. D., Brown, J., and Dickson, R. R. (1999). Frontal structure and Antarctic Bottom Water flow through the Princess Elizabeth Trough, Antarctica. *Deep Sea Res. Part I: Oceanographic Res. Papers* 46 (7), 1181–1200. doi: 10.1016/S0967-0637(98)00108-3

Hillenbrand, C.-D., Smith, J. A., Kuhn, G., Esper, O., Gersonde, R., Larter, R. D., et al. (2010). Age assignment of a diatomaceous ooze deposited in the western Amundsen Sea Embayment after the Last Glacial Maximum. *J. Quat. Sci.* 25 (3), 280–295. doi: 10.1002/jqs.1308

Hoogakker, B. A. A., Elderfield, H., Schmiedl, G., McCave, I. N., and Rickaby, R. E. M. (2015). Glacial–interglacial changes in bottom-water oxygen content on the Portuguese margin. *Nat. Geosci.* 8 (1), 40–43. doi: 10.1038/ngeo2317

Hu, B.-Y., Long, F.-J., Han, X.-B., Zhang, Y.-C., Hu, L.-M., Xiang, B., et al. (2022). The evolution of paleoproductivity since the Middle Holocene in the Cosmonaut Sea, Antarctic. *Earth Sci. Front.* 29 (4), 113–122. doi: 10.13745/j.esf.sf.2022.1.12

Hunt, B. P. V., Pakhomov, E. A., and Trotsenko, B. G. (2007). The macrozooplankton of the Cosmonaut Sea, east Antarctica (30°E–60°E), 1987–1990. *Deep Sea Res. Part I: Oceanographic Res. Papers* 54 (7), 1042–1069. doi: 10.1016/j.dsr.2007.04.002

Jaccard, S. L., and Galbraith, E. D. (2012). Large climate-driven changes of oceanic oxygen concentrations during the last deglaciation. *Nat. Geosci.* 5 (2), 151–156. doi: 10.1038/ngeo1352

Jaccard, S. L., Galbraith, E. D., Martínez-García, A., and Anderson, R. F. (2016). Covariation of deep Southern Ocean oxygenation and atmospheric CO_2 through the last ice age. *Nature* 530 (7589), 207–210. doi: 10.1038/nature16514

Jaccard, S. L., Haug, G. H., Sigman, D. M., Pedersen, T. F., Thierstein, H. R., and Röhl, U. (2005). Glacial/interglacial changes in subarctic north pacific stratification. *Science* 308 (5724), 1003–1006. doi: 10.1126/science.1108696

Jaccard, S. L., Hayes, C. T., Martínez-García, A., Hodell, D. A., Anderson, R. F., Sigman, D. M., et al. (2013). Two modes of change in southern ocean productivity over the past million years. *Science* 339 (6126), 1419–1423. doi: 10.1126/science.1227545

Jacobel, A. W., McManus, J. F., Anderson, R. F., and Winckler, G. (2017). Repeated storage of respired carbon in the equatorial Pacific Ocean over the last three glacial cycles. *Nat. Commun.* 8 (1), 1727. doi: 10.1038/s41467-017-01938-x

Jae Il, L., Bak, Y.-S., Yoo, K.-C., Hyoun Soo, L., Ho Il, Y., and Suk Hee, Y. (2010). Climate changes in the South Orkney Plateau during the last 8600 years. *Holocene* 20 (3), 395–404. doi: 10.1177/0959683609353430

Jena, B., and Pillai, A. N. (2020). Satellite observations of unprecedented phytoplankton blooms in the Maud Rise polynya, Southern Ocean. *Cryosphere* 14 (4), 1385–1398. doi: 10.5194/tc-14-1385-2020

Keir, R. S. (1988). On the Late Pleistocene ocean geochemistry and circulation. *Paleoceanography* 3 (4), 413–445. doi: 10.1029/PA003i004p00413

Kim, S., Yoo, K.-C., Lee, J. I., Roh, Y. H., Bak, Y.-S., Um, I.-K., et al. (2020). Paleoceanographic changes in the Southern Ocean off Elephant Island since the last

glacial period: Links between surface water productivity, nutrient utilization, bottom water currents, and ice-rafted debris. *Quat. Sci. Rev.* 249, 106563. doi: 10.1016/j.quascirev.2020.106563

Klyausov, A. V., and Lanin, V. I. (1988). "On the near-shelf frontal zone in the Commonwealth and Cosmonaut Seas," in *Interdisciplinary investigations of pelagic ecosystem in the commonwealth and cosmonaut seas*. Eds. T. G. Lubimova, R. R. Makarov, V. V. Maslennikov, E. Z. Samyshev, V. A. Bibik and T. G. Tarverdieva (Moscow: VNIRO Publishers), 56–62.

Kohfeld, K. E., Quéré, C. L., Harrison, S. P., and Anderson, R. F. (2005). Role of marine biology in glacial-interglacial CO_2 cycles. *Science* 308 (5718), 74–78. doi: 10.1126/science.1105375

Kopczyńska, E. E., Goeyens, L., Semeneh, M., and Dehairs, F. (1995). Phytoplankton composition and cell carbon distribution in Prydz Bay, Antarctica: relation to organic particulate matter and its $\delta^{13}C$ values. *J. Plankton Res.* 17 (4), 685–707. doi: 10.1093/plankt/17.4.685

Kulbe, T., Melles, M., Verkulich, S. R., and Pushina, Z. V. (2001). East antarctic climate and environmental variability over the last 9400 years inferred from marine sediments of the bunger oasis. *Arctic Antarctic Alpine Res.* 33 (2), 223–230. doi: 10.2307/1552223

Langmuir, D. (1978). Uranium solution-mineral equilibria at low temperatures with applications to sedimentary ore deposits. *Geochimica Cosmochimica Acta* 42 (6, Part A), 547–569. doi: 10.1016/0016-7037(78)90001-7

Laskar, J., Robutel, P., Joutel, F., Gastineau, M., Correia, A. C. M., and Levrard, B. (2004). A long-term numerical solution for the insolation quantities of the Earth. *Astronomy Astrophysics* 428, 261–285. doi: 10.1051/0004-6361:20041335

Learman, D. R., Henson, M. W., Thrash, J. C., Temperton, B., Brannock, P. M., Santos, S. R., et al. (2016). Biogeochemical and Microbial Variation across 5500 km of Antarctic Surface Sediment Implicates Organic Matter as a Driver of Benthic Community Structure. *Front. Microbiol.* 7. doi: 10.3389/fmicb.2016.00284

Lei, Z.-Y., Ge, Q., Chen, D., Zhang, Y.-C., Han, X.-B., Ye, L.-M., et al. (2021). The paleoclimatic significance and sources of sediments from the Amundsen Sea in West Antarctic since Mid-Holocene. *Earth Sci. Front.* 29 (4), 179–190. doi: 10.13745/j.esf.sf.2022.1.7

Li, C., Love, G. D., Lyons, T. W., Fike, D. A., Sessions, A. L., and Chu, X.-L. (2010). A stratified redox model for the ediacaran ocean. *Science* 328 (5974), 80–83. doi: 10.1126/science.1182369

Li, Q.-M., Xiao, W.-S., Wang, R.-J., and Chen, Z.-H. (2021). Diatom based reconstruction of climate evolution through the Last Glacial Maximum to Holocene in the Cosmonaut Sea, East Antarctica. *Deep Sea Res. Part II: Topical Stud. Oceanography* 194, 104960. doi: 10.1016/j.dsr2.2021.104960

Licht, K. J., and Andrews, J. T. (2002). The ^{14}C record of late pleistocene ice advance and retreat in the central ross sea, Antarctica. *Arctic Antarctic Alpine Res.* 34, 324–333.

Lin, H.-L., Lai, C.-T., Ting, H.-C., Wang, L., Sarnthein, M., and Hung, J.-J. (1999). Late Pleistocene nutrients and sea surface productivity in the South China Sea: a record of teleconnections with Northern hemisphere events. *Mar. Geol.* 156 (1), 197–210. doi: 10.1016/S0025-3227(98)00179-0

Liu, H.-L., Chen, Z.-H., Ge, S.-L., Xiao, W.-S., Wang, H.-Z., Tang, Z., et al. (2015). Late Quaternary sedimentary records and paleoceanographic implications from the core on continental slope off the Prydz Bay, East Antarctic. *Mar. Geology Quaternary Geology* 35 (03), 209–217. doi: 10.3724/SP.J.1140.2015.03209

Liu, R.-J., Yu, P.-S., Hu, C.-Y., Han, Z.-B., and Pan, J.-M. (2014). Contents and distributions of organic carbon and total nitrogen in sediments of Prydz Bay, Antarctic. *Acta Oceanologica Sin.* 36 (4), 118–125.

Macko, S. A., and Estep, M. L. F. (1984). Microbial alteration of stable nitrogen and carbon isotopic compositions of organic matter. *Org. Geochem.* 6, 787–790. doi: 10.1016/01466380(84)90100-1

Macko, S., and Pereira, C. (1990). Neogene paleoclimate development of the antarctic weddell sea region: Organic geochemistry. *Proceedings of the Ocean Drilling Program, Scientific Results* 113, 881–897. doi: 10.2973/odp.proc.sr.113.190.1990

Matsumoto, K. (2007). Biology-mediated temperature control on atmospheric pCO2 and ocean biogeochemistry. *Geophys. Res. Lett.* 34 (20), L20605. doi: 10.1029/2007GL031301

McManus, J., Berelson, W. M., Klinkhammer, G. P., Johnson, K. S., Coale, K. H., Anderson, R. F., et al. (1998). Geochemistry of barium in marine sediments: implications for its use as a paleoproxy. *Geochimica Cosmochimica Acta* 62 (21), 3453–3473. doi: 10.1016/S0016-7037(98)00248-8

McManus, J. F., Francois, R., Gherardi, J. M., Keigwin, L. D., and Brown-Leger, S. (2004). Collapse and rapid resumption of Atlantic meridional circulation linked to deglacial climate changes. *Nature* 428 (6985), 834–837. doi: 10.1038/nature02494

Mei, J., Wang, R.-J., Zhang, T.-L., Xiao, W.-S., Chen, Z.-H., Chen, J.-F., et al. (2015). Paleoceanopraphic records of core 08P31 on the Chukchi Plateau, Weatern Arctic Ocean. *Haiyang Xuebao* 37 (5), 121–135. doi: 10.3969/j.issn.0253-4193.2015.05.012

Meijers, A. J. S., Klocker, A., Bindoff, N. L., Williams, G. D., and Marsland, S. J. (2010). The circulation and water masses of the Antarctic shelf and continental slope between 30 and 80°E. *Deep Sea Res. Part II: Topical Stud. Oceanography* 57 (9), 723–737. doi: 10.1016/j.dsr2.2009.04.019

Meyers, P. A. (1997). Organic geochemical proxies of paleoceanographic, paleolimnologic, and paleoclimatic processes. *Org. Geochem.* 27 (5), 213–250. doi: 10.1016/S0146-6380(97)00049-1

Middelburg, J. J., De Lange, G. J., and van der Weijden, C. H. (1987). Manganese solubility control in marine pore waters. *Geochimica Cosmochimica Acta* 51 (3), 759–763. doi: 10.1016/0016-7037(87)90086-X

Monnin, E., Steig, E. J., Siegenthaler, U., Kawamura, K., Schwander, J., Stauffer, B., et al. (2004). Evidence for substantial accumulation rate variability in Antarctica during the Holocene, through synchronization of CO_2 in the Taylor Dome, Dome C and DML ice cores. *Earth Planetary Sci. Lett.* 224 (1), 45–54. doi: 10.1016/j.epsl.2004.05.007

Moore, J. K., and Abbott, M. R. (2000). Phytoplankton chlorophyll distributions and primary production in the Southern Ocean. *J. Geophysical Research: Oceans* 105 (C12), 28709–28722. doi: 10.1029/1999JC000043

Morales Maqueda, M. A., Willmott, A. J., and Biggs, N. R. T. (2004). Polynya dynamics: A review of observations and modeling. *Rev. Geophysics* 42 (1), RG1004. doi: 10.1029/2002RG000116

Morford, J. L., and Emerson, S. (1999). The geochemistry of redox sensitive trace metals in sediments. *Geochimica Cosmochimica Acta* 63 (11), 1735–1750. doi: 10.1016/S0016-7037(99)00126-X

Morford, J. L., Russell, A. D., and Emerson, S. (2001). Trace metal evidence for changes in the redox environment associated with the transition from terrigenous clay to diatomaceous sediment, Saanich Inlet, BC. *Mar. Geol.* 174 (1), 355–369. doi: 10.1016/S0025-3227(00)00160-2

Nameroff, T. J., Balistrieri, L. S., and Murray, J. W. (2002). Suboxic trace metal geochemistry in the Eastern Tropical North Pacific. *Geochimica Cosmochimica Acta* 66 (7), 1139–1158. doi: 10.1016/S0016-7037(01)00843-2

Nelson, D. M., Tréguer, P., Brzezinski, M. A., Leynaert, A., and Quéguiner, B. (1995). Production and dissolution of biogenic silica in the ocean: Revised global estimates, comparison with regional data and relationship to biogenic sedimentation. *Glob. Biogeochem. Cycles* 9 (3), 359–372. doi: 10.1029/95GB01070

Nicol, S., and Foster, J. (2003). Recent trends in the fishery for Antarctic krill. *Aquat. Living Resour.* 16 (1), 42–45. doi: 10.1016/S0990-7440(03)00004-4

Ogrinc, N., Fontolan, G., Faganeli, J., and Covelli, S. (2005). Carbon and nitrogen isotope compositions of organic matter in coastal marine sediments (the Gulf of Trieste, N Adriatic Sea): indicators of sources and preservation. *Mar. Chem.* 95 (3), 163–181. doi: 10.1016/j.marchem.2004.09.003

Orme, L. C., Crosta, X., Miettinen, A., Divine, D. V., Husum, K., Isaksson, E., et al. (2020). Sea surface temperature in the Indian sector of the Southern Ocean over the Late Glacial and Holocene. *Clim. Past* 16 (4), 1451–1467. doi: 10.5194/cp-16-1451-2020

Orsi, A. H., Whitworth, T., and Nowlin, W. D. (1995). On the meridional extent and fronts of the Antarctic Circumpolar Current. *Deep Sea Res. Part I: Oceanographic Res. Papers* 42 (5), 641–673. doi: 10.1016/0967-0637(95)00021-W

Pailler, D., Bard, E., Rostek, F., Zheng, Y., Mortlock, R., and van Geen, A. (2002). Burial of redox- metals and organic matter in the equatorial Indian Ocean linked to precession. *Geochimica Cosmochimica Acta* 66 (5), 849–865. doi: 10.1016/S0016-7037(01)00817-1

Paytan, A., Kastner, M., and Chavez, F. P. (1996). Glacial to interglacial fluctuations in productivity in the equatorial pacific as indicated by marine barite. *Science* 274 (5291), 1355. doi: 10.1126/science.274.5291.1355

Prahl, F. G., Ertel, J. R., Goni, M. A., Sparrow, M. A., and Eversmeyer, B. (1994). Terrestrial organic carbon contributions to sediments on the Washington margin. *Geochimica Cosmochimica Acta* 58 (14), 3035–3048. doi: 10.1016/0016-7037(94)90177-5

Prasad, T. G., McClean, J. L., Hunke, E. C., Semtner, A. J., and Ivanova, D. (2005). A numerical study of the western Cosmonaut polynya in a coupled ocean–sea ice model. *J. Geophysical Research: Oceans* 110 (C10), C10008. doi: 10.1029/2004JC002858

Pudsey, C. J., Murray, J. W., Appleby, P., and Evans, J. (2006). Ice shelf history from petrographic and foraminiferal evidence, Northeast Antarctic Peninsula. *Quaternary Sci. Rev.* 25 (17), 2357–2379. doi: 10.1016/j.quascirev.2006.01.029

Quéguiner, B., Tréguer, P., and Nelson, D. M. (1991). The production of biogenic silica in the Weddell and Scotia Seas. *Mar. Chem.* 35 (1), 449–459. doi: 10.1016/S0304-4203(09)90036-6

Rae, J. W. B., Burke, A., Robinson, L. F., Adkins, J. F., Chen, T., Cole, C., et al. (2018). CO_2 storage and release in the deep Southern Ocean on millennial to centennial timescales. *Nature* 562 (7728), 569–573. doi: 10.1038/s41586-018-0614-0

Raynaud, D., Barnola, J. M., Chappellaz, J., Zardini, D., Jouzel, J., and Lorius, C. (1992). Glacial-interglacial evolution of greenhouse gases as inferred from ice core analysis: A review of recent results. *Quat. Sci. Rev.* 11 (4), 381–386. doi: 10.1016/0277-3791(92)90020-9

Ridgwell, A., and Schmidt, D. N. (2010). Past constraints on the vulnerability of marine calcifiers to massive carbon dioxide release. *Nat. Geosci.* 3 (3), 196–200. doi: 10.1038/ngeo755

Robinson, R. S., Kienast, M., Luiza Albuquerque, A., Altabet, M., Contreras, S., De Pol Holz, R., et al. (2012). A review of nitrogen isotopic alteration in marine sediments. *Paleoceanography* 27 (4), PA4203. doi: 10.1029/2012PA002321

Sampei, Y., and Matsumoto, E. (2001). C/N ratios in a sediment core from Nakaumi Lagoon, southwest Japan - Usefulness as an organic source indicator -. *Geochem. J.* 35 (3), 189–205. doi: 10.2343/geochemj.35.189

Sarmiento, J. L., and Nicolas, G. (2006). *Ocean biogeochemical dynamics* (Princeton: Princeton University Press). doi: 10.2307/j.ctt3fgxqx

Sarnthein, M., Schneider, B., and Grootes, P. M. (2013). Peak glacial ^{14}C ventilation ages suggest major draw-down of carbon into the abyssal ocean. *Climate Past* 9 (6), 2595–2614. doi: 10.5194/cp-9-2595-2013

Schmitt, J., Schneider, R., Elsig, J., Leuenberger, D., Lourantou, A., Chappellaz, J., et al. (2012). Carbon isotope constraints on the deglacial CO_2 rise from ice cores. *Science* 336 (6082), 711–714. doi: 10.1126/science.1217161

Schmittner, A., Oschlies, A., Matthews, H. D., and Galbraith, E. D. (2008). Future changes in climate, ocean circulation, ecosystems, and biogeochemical cycling simulated for a business-as-usual CO_2 emission scenario until year 4000 AD. *Glob. Biogeochem. Cycles* 22 (1), GB1013. doi: 10.1029/2007GB002953

Schüpbach, S., Federer, U., Kaufmann, P., Albani, S., Barbante, C., Stocker, T., et al. (2013). High-resolution mineral dust and sea ice proxy records from the Talos Dome ice core. *Climate Past* 9, 2789–2807. doi: 10.5194/cp-9-2789-2013

Shakun, J. D., Clark, P. U., He, F., Marcott, S. A., Mix, A. C., Liu, Z., et al. (2012). Global warming preceded by increasing carbon dioxide concentrations during the last deglaciation. *Nature* 484 (7392), 49–54. doi: 10.1038/nature10915

Siani, G., Michel, E., De Pol-Holz, R., DeVries, T., Lamy, F., Carel, M., et al. (2013). Carbon isotope records reveal precise timing of enhanced Southern Ocean upwelling during the last deglaciation. *Nat. Commun.* 4 (1), 2758. doi: 10.1038/ncomms3758

Sigman, D. M., and Boyle, E. A. (2000). Glacial/interglacial variations in atmospheric carbon dioxide. *Nature* 407 (6806), 859–869. doi: 10.1038/35038000

Sigman, D. M., Fripiat, F., Studer, A. S., Kemeny, P. C., Martínez-García, A., Hain, M. P., et al. (2021). The Southern Ocean during the ice ages: A review of the Antarctic surface isolation hypothesis, with comparison to the North Pacific. *Quat. Sci. Rev.* 254, 106732. doi: 10.1016/j.quascirev.2020.106732

Sigman, D. M., Hain, M. P., and Haug, G. H. (2010). The polar ocean and glacial cycles in atmospheric CO_2 concentration. *Nature* 466 (7302), 47–55. doi: 10.1038/nature09149

Skinner, L. C., Fallon, S., Waelbroeck, C., Michel, E., and Barker, S. (2010). Ventilation of the deep southern ocean and deglacial CO_2 rise. *Science* 328 (5982), 1147–1151. doi: 10.1126/science.1183627

Skinner, L. C., Primeau, F., Freeman, E., de la Fuente, M., Goodwin, P. A., Gottschalk, J., et al. (2017). Radiocarbon constraints on the glacial ocean circulation and its impact on atmospheric CO_2. *Nat. Commun.* 8 (1), 16010. doi: 10.1038/ncomms16010

Smith, W. O. (1991). Nutrient distributions and new production in polar regions: parallels and contrasts between the Arctic and Antarctic. *Mar. Chem.* 35 (1), 245–257. doi: 10.1016/S0304-4203(09)90020-2

Smith, S. D., Muench, R. D., and Pease, C. H. (1990). Polynyas and leads: An overview of physical processes and environment. *J. Geophysical Research: Oceans* 95 (C6), 9461–9479. doi: 10.1029/JC095iC06p09461

Strauch, G., Haendel, D., Maass, I., Mühle, K., and Runge, A. (2011). Isotope variations of hydrogen, carbon and nitrogen in florae from the Schirmacher Oasis, East Antarctica. *Isotopes Environ. Health Stud.* 47 (3), 280–285. doi: 10.1080/10256016.2011.600455

Stroobants, N., Dehairs, F., Goeyens, L., Vanderheijden, N., and Van Grieken, R. (1991). Barite formation in the Southern Ocean water column. *Mar. Chem.* 35 (1), 411–421. doi: 10.1016/S0304-4203(09)90033-0

Studer, A. S., Sigman, D. M., Martínez-García, A., Benz, V., Winckler, G., Kuhn, G., et al. (2015). Antarctic Zone nutrient conditions during the last two glacial cycles. *Paleoceanography* 30 (7), 845–862. doi: 10.1002/2014PA002745

Stuiver, M., and Reimer, P. J. (1993). Extended ^{14}C data base and revised CALIB 3.0 ^{14}C age calibration program. *Radiocarbon* 35 (1), 215–230. doi: 10.1017/S0033822200013904

Takano, Y., Tyler, J. J., Kojima, H., Yokoyama, Y., Tanabe, Y., Sato, T., et al. (2012). Holocene lake development and glacial-isostatic uplift at Lake Skallen and Lake Oyako, Lützow-Holm Bay, East Antarctica: Based on biogeochemical facies and molecular signatures. *Appl. Geochem.* 27 (12), 2546–2559. doi: 10.1016/j.apgeochem.2012.08.009

Talley, L. D. (2013). Closure of the global overturning circulation through the Indian, Pacific, and Southern Oceans: Schematics and transports. *Oceanography* 26 (1), 80–97. doi: 10.5670/oceanog.2013.07

Thöle, L. M., Amsler, H. E., Moretti, S., Auderset, A., Gilgannon, J., Lippold, J., et al. (2019). Glacial-interglacial dust and export production records from the Southern Indian Ocean. *Earth Planetary Sci. Lett.* 525, 115716. doi: 10.1016/j.epsl.2019.115716

Thornton, S. F., and McManus, J. (1994). Application of organic carbon and nitrogen stable isotope and C/N ratios as source indicators of organic matter provenance in estuarine systems: Evidence from the tay estuary, scotland. *Estuarine Coast. Shelf Sci.* 38 (3), 219–233. doi: 10.1006/ecss.1994.1015

Thunell, R. C., Miao, Q.-M., Calvert, S. E., and Pedersen, T. F. (1992). Glacial-holocene biogenic sedimentation patterns in the South China sea: Productivity variations and surface water pCO_2. *Paleoceanography* 7 (2), 143–162. doi: 10.1029/92PA00278

Toggweiler, J. R. (1999). Variation of atmospheric CO2 by ventilation of the ocean's deepest water. *Paleoceanography* 14 (5), 571–588. doi: 10.1029/1999PA900033

Toggweiler, J. R., Russell, J. L., and Carson, S. R. (2006). Midlatitude westerlies, atmospheric CO_2, and climate change during the ice ages. *Paleoceanography* 21 (2), PA2005. doi: 10.1029/2005PA001154

Tréguer, P. (2002). Silica and the cycle of carbon in the ocean. *Comptes Rendus Geosci.* 334 (1), 3–11. doi: 10.1016/S1631-0713(02)01680-2

Tribovillard, N., Algeo, T. J., Lyons, T., and Riboulleau, A. (2006). Trace metals as paleoredox and paleoproductivity proxies: An update. *Chem. Geol.* 232 (1), 12–32. doi: 10.1016/j.chemgeo.2006.02.012

Turekian, K. K., and Wedepohl, K. H. (1961). Distribution of the elements in some major units of the earth's crust. *GSA Bull.* 72 (2), 175–192. doi: 10.1130/0016-7606(1961)72[175:DOTEIS]2.0.CO;2

von Berg, L., Prend, C. J., Campbell, E. C., Mazloff, M. R., Talley, L. D., and Gille, S. T. (2020). Weddell sea phytoplankton blooms modulated by sea ice variability and polynya formation. *Geophys. Res. Lett.* 47 (11), e2020GL087954. doi: 10.1029/2020GL087954

Wang, J.-K., Li, T.-G., Xiong, Z.-F., Chang, F.-M., Qin, B.-B., Wang, L.-M., et al. (2018). Sedimentary geochemical characteristics of the Redox-sensitive elements in Ross Sea, Antarctic: Implications for paleoceanography. *Mar. Geology Quaternary Geology* 38 (5), 112–121. doi: 10.16562/j.cnki.0256-1492.2018.05.011

Watson, A. J., and Naveira Garabato, A. C. (2006). The role of Southern Ocean mixing and upwelling in glacial-interglacial atmospheric CO_2 change. *Tellus B* 58 (1), 73–87. doi: 10.1111/j.1600-0889.2005.00167.x

Watson, A. J., Vallis, G. K., and Nikurashin, M. (2015). Southern Ocean buoyancy forcing of ocean ventilation and glacial atmospheric CO_2. *Nat. Geosci.* 8 (11), 861–864. doi: 10.1038/ngeo2538

Westwood, K. J., Brian Griffiths, F., Meiners, K. M., and Williams, G. D. (2010). Primary productivity off the Antarctic coast from 30°–80°E; BROKE-West surve. *Deep Sea Res. Part II: Topical Stud. Oceanography* 57 (9), 794–814. doi: 10.1016/j.dsr2.2008.08.020

Williams, G. D., Nicol, S., Aoki, S., Meijers, A. J. S., Bindoff, N. L., Iijima, Y., et al. (2010). Surface oceanography of BROKE-West, along the Antarctic margin of the south-west Indian Ocean (30–80°E). *Deep Sea Res. Part II: Topical Stud. Oceanography* 57 (9), 738–757. doi: 10.1016/j.dsr2.2009.04.020

Wolff, E. W., Barbante, C., Becagli, S., Bigler, M., Boutron, C. F., Castellano, E., et al. (2010). Changes in environment over the last 800,000 years from chemical analysis of the EPICA Dome C ice core. *Quat. Sci. Rev.* 29 (1), 285–295. doi: 10.1016/j.quascirev.2009.06.013

Wolff, E. W., Fischer, H., Fundel, F., Ruth, U., Twarloh, B., Littot, G. C., et al. (2006). Southern Ocean sea-ice extent, productivity and iron flux over the past eight glacial cycles. *Nature* 440 (7083), 491–496. doi: 10.1038/nature04614

Wong, A. P. S., Bindoff, N. L., and Forbes, A. (1985). "Ocean-ice shelf interaction and possible bottom water formation in prydz bay, Antarctica," in *Ocean, ice, and atmosphere: Interactions at the antarctic continental margin*. Eds. S. S. Jacobs and R. F. Weiss (Washington, DC: American Geophysical Union), 173–187.

Yamamoto, A., Abe-Ouchi, A., Shigemitsu, M., Oka, A., Takahashi, K., Ohgaito, R., et al. (2015). Global deep ocean oxygenation by enhanced ventilation in the Southern Ocean under long-term global warming. *Glob. Biogeochem. Cycles* 29 (10), 1801–1815. doi: 10.1002/2015GB005181

Yang, Z.-F., Chen, M., Tang, Z., Zheng, M.-F., and Qiu, Y.-S. (2022). The sedimentation, bioturbation and organic matter degradation as revealed by excess ^{230}Th and ^{210}Pb in the Cosmonaut Sea. *Deep Sea Res. Part II: Topical Stud. Oceanography* 198, 105049. doi: 10.1016/j.dsr2.2022.105049

Yang, C.-L., Chen, Z.-H., Xiao, W.-S., Wang, X., Ju, M.-S., Cui, Y.-C., et al. (2021). Paleoproductivity and its environmental constraints in the Scotia Sea, Antarctica since 34 ka BP. *Haiyang Xuebao* 43 (03), 116–125. doi: 10.12284/hyxb2021051

Yoshida, Y., and Moriwaki, K. (1979). Some consideration on elevated coastal features and their dates around syowa station, Antarctica. *Memoirs Natl. Institute Polar Res. Special issue* 13, 220–226.

Zhang, Y., Li, C.-L., Yang, G., Wang, Y.-Q., Tao, Z.-C., Zhang, Y.-S., et al. (2017). Ontogenetic diet shift in Antarctic krill (Euphausia superba) in the Prydz Bay: A stable isotope analysis. *Acta Oceanologica Sin.* 36 (12), 67–78. doi: 10.1007/s13131-017-1049-4